APPLICATION OF COMPUTATIONAL INTELLIGENCE FOR FAULT DETECTION AND DIAGNOSIS OF INDUCTION MOTORS AND ELECTROMECHANICAL SYSTEMS

ZHANG YIFAN

NATIONAL UNIVERSITY OF SINGAPORE

2012

APPLICATION OF COMPUTATIONAL INTELLIGENCE FOR FAULT DETECTION AND DIAGNOSIS OF INDUCTION MOTORS AND ELECTROMECHANICAL SYSTEMS

ZHANG YIFAN

B. Eng. (Hons.), Tianjin University

A THESIS SUBMITTED

FOR THE DEGREE OF MASTER OF ENGINEERING

DEPARTMENT OF ELECTRICAL AND COMPUTER ENGINEERING

NATIONAL UNIVERSITY OF SINGAPORE

2012

DECLARATION

I hereby declare that the thesis is my original work and it has been written by me in its entirety.
I have duly acknowledged all the sources of information which have been used in the thesis.

This thesis has also not been submitted for any degree in any university previously.

_____

ZHANG YIFAN

September 2012

ACKNOWLEDGEMENTS

First of all, I would like to express my deep and hearty gratitude to my supervisor, A/Prof Chang Che Sau, whose invaluable encouragement, support and guidance throughout my Engineer Master studies ensured me to develop a better understanding of the project, overcome all the difficulties in the research, and finally finish this thesis. Without his insightful advices and constant help, this thesis would not have been possible.

I would like to acknowledge research fellow, Dr. Wang Zhaoxia, for her kind support and knowledge transfer of FFT and ICA.

I am also thankful to research engineer, Miss Lu Wenjing, for her many generous help and constructive discussions in my research.

I want to take this chance to thank the technologist-in-charge of the Power Systems Laboratory, Mr. Seow Hung Cheng, for organizing seminar with our external co-worker, maintaining of laboratory equipment and providing assistance.

I wish to thank research engineer, Miss Wu Di, for her immense knowledge, motivation and enthusiasm, which help me in my study and life in Singapore.

Finally, I would like to sincerely thank my friends and family for their endless, unconditional, and dedicated love and constant support.

TABLE OF CONTENTS

SUMMARY i

LIST OF TABLES iii

LIST OF FIGURES iv

LIST OF SYMBOLS AND ABBREVIATIONS vi

CHAPTER 1 INTRODUCTION 10

1.1 Motivations and Objectives 10

1.2 Previous Work and Contributions of This Thesis 12

1.3 Thesis Outline 15

CHAPTER 2 INDUCTION MOTOR AND DATA COLLECTION 19

2.1 Introduction 19

2.1.1 Structure of Induction Motor 19

2.1.2 Basic Operation of Induction Motor 22

2.2 Fault Specifications 24

2.3 Data Collection 25

2.3.1 Data from CWRU [8] 25

2.3.2 Data from Vestas 28

2.3.3 Data from SKF 29

CHAPTER 3 SIGNATURE FEATURE EXTRACTION 30

3.1 Theoretical Analysis of the Proposed FFT 30

3.2 Envelope Analysis 34

3.2.1 Steps of the Envelope Analysis 35

3.2.2 Definition of Hilbert Transformation 35

3.2.3 Demodulation Principle of Hilbert Transformation 36

3.3 Vibration Data Processing 37

3.3.1 Data Processing for CWRU [8] 38

3.3.2 Data Processing for Vestas 42

3.3.3 Data Processing for SKF Data Sets 44
CHAPTER 4 INDEPENDENT COMPONENT ANALYSIS 46
4.1 Introduction 46
4.1.1 Independence in ICA 48
4.1.2 Data Preprocessing for ICA 50
4.1.3 Fast-ICA 52
4.1.4 Formulation of the FastICA 53
4.2 Feature Extraction and ICA Plot 56
4.2.1 ICA Plot of CWRU Data sets [8] 57
4.2.2 ICA Plot of Vestas sets 58
4.2.3 ICA Plot of SKF Data sets 59
CHAPTER 5 SUPPORT VECTOR MACHINE 61
5.1 Introduction 61
5.1.1 Data Preparation for SVM 61
5.1.2 Classification of SVM 62
5.2 Training and Classification 66
CHAPTER 6 PROPOSED FAULT CLASSIFICATION PLATFORM AND RESULTS 70
6.1 System Scheme 70
6.2 Project Results and Discussion 71
6.2.1 Summary of Results for CWRU [8] 71
6.2.2 Results for Vestas 75
6.2.3 Results for SKF data sets 77
CHAPTER 7 CONCLUSION 79
7.1 Outcomes 79
7.2 Future Work 80
APPENDICES 82
A.1 CWRU Vibration data Information [8] 82
A.2 MATLAB Source Codes 84

A.2.1 FFT.m 84
A.2.2 EnvelopAnalysis.m 85
A.2.3 SVM.m 85
A.2.4 ICA_Pre-Processing.m 87
A.2.5 ICA_Feature_Extraction.m 87
REFERENCES 89

SUMMARY

Induction motors are widely used in industries. However, online predictive detection and diagnosis of mechanical faults of an induction motor is still a challenging problem. The increasing economic pressure has required the development of a cost-effective maintenance system to guarantee induction operating reliability and relatively low cost. Therefore, it is crucially important to develop intelligent tools to detect and diagnose mechanical faults for the reliable operation of induction motor systems. This thesis aims at studying this issue and proposing effective solutions. The major contributions of the thesis are:

Fast Fourier Transform (FFT) is known to be an efficient algorithm of computing the Discrete Fourier Transform (DFT) [1], which decomposes a vibration signal of time domain into frequency domain and is generally used in digital signal processing. Furthermore, Envelope Analysis is an algorithm to translate a signal into Intrinsic Mode Functions (IMF) and gain instantaneous frequency data. The new design combines these two algorithms and proposes a hybrid method, named as FFT-En, which translates vibration signal of induction motors from time domain to frequency domain, and then using Envelope Analysis significantly reduces the influence of noise and effectively extracts the fault signals.

Independent Component Analysis (ICA) is developed to separate a multivariate blind signal source into additive subcomponents, which assumes that the source signals are non-Gaussian mutual statistical independence signals. ICA is widely applied in load estimation of power systems, image processing, and biomedical engineering areas.

However, ICA is rarely applied to detect induction motors fault. The new design utilizes ICA to perform reliable diagnosis and applied Support Vector Machine (SVM) to sort the ICA results for classification and regression analysis. The new design is shown to have outperformed previously reported algorithms by significantly increasing the speed and accuracy of predictive detection and diagnosis of induction motors mechanical faults.

LIST OF TABLES

Table No.	Table Title	Page No.
Table 2.3.1-a)	Defect frequencies: (multiple of running speed in Hz) [8]	25
Table 2.3.1-b)	Drive-end bearing-fault specifications (1 mil=0.001 inches) [8]	26
Table 2.3.1-c)	Fan-end bearing-fault specifications (1 mil=0.001 inches) [8]	27
Table 2.3.1-d)	Normal baseline data [8]	27
Table 2.3.2	Vestas in Singapore vibration data record list	28
Table 6.2.1	Accuracy of fault classification using SVM (%)	71
Table A.1-a)	12k drive-end bearing-fault data	82
Table A.1-b)	48k drive-end bearing-fault data	83
Table A.1-c)	12k fan-end bearing-fault data	83

LIST OF FIGURES

Fig. No.	Figure Title	Page No.
Fig. 1.1	A typical system of induction motor fault detection	11
Fig. 1.2	Proposed automatic motor fault detection and diagnosis scheme	16
Fig. 2.1.1-a)	Structure of an induction motor [5]	19
Fig. 2.1.1-b)	The stator of an induction motor [6]	20
Fig. 2.1.1-c)	The rotor of an induction motor [6]	21
Fig. 2.1.1-d)	Partially assembled motor [6]	21
Fig. 2.1.2-a)	A 3-phase stator [7]	22
Fig. 2.1.2-b)	360 degree rotation [7]	23
Fig. 2.2	Fault located on the bearing	24
Fig. 2.3.1	Test stand [8]	26
Fig. 3.1	The process of DFT and Inverse DFT	31
Fig. 3.2.1	Steps of Envelope Analysis diagnosis	35
Fig. 3.3.1-a)	FFT-En plot of normal bearing	38
Fig. 3.3.1-b)	FFT-En plot of ball—fault bearing	39
Fig. 3.3.1-c)	FFT-En plot of inner race fault Bearing	40
Fig. 3.3.1-d)	FFT-En plot of outer race fault bearing @3 o'clock	40
Fig. 3.3.1-e)	FFT-En plot of outer race fault bearing @6 o'clock	41
Fig. 3.3.1-f)	FFT-En plot of outer race fault bearing @12 o'clock	41
Fig. 3.3.2-a)	FFT-En plot of a broken Vestas wind turbine	42
Fig. 3.3.2-b)	FFT-En plot of a health Vestas wind turbine	43
Fig. 3.3.3-a)	FFT-En plot of a health motor SKF Bearing	44

Fig. 3.3.3-b) FFT-En plot of a damaged SKF bearing 45

Fig. 4.1.2-a) The signal with normal condition before and after preprocessing 51

Fig. 4.1.2-b) The signal with bearing-fault before and after preprocessing 51

Fig. 4.2.1 ICA plot for CWRU data sets 57

Fig. 4.2.2 ICA plot for Vestas data sets 58

Fig. 4.2.3 ICA plot for SKF data sets 59

Fig. 5.1.2-a) Steps of classification of SVM 63

Fig. 5.1.2-b) Classification using SVM 63

Fig. 5.2-a) SVM plot of training set 67

Fig. 5.2-b) Zoom plot of training set SVM result 68

Fig. 5.2-c) SVM plot of test set 68

Fig. 5.2-d) Zoom plot of test set SVM result 69

Fig. 6.2.1-a) SVM plot for training set 72

Fig. 6.2.1-b) SVM plot for test set 73

Fig. 6.2.1-c) Zoom of SVM plot for test set 74

Fig. 6.2.2-a) Classification of Vestas data sets using ICA 75

Fig. 6.2.2-b) Classification of Vestas data sets using ICA in 3dimension 76

Fig. 6.2.3-a) Classification of SKF data sets using FFT-En-ICA 77

Fig. 6.2.3-b) Classification of SKF data sets only using FFT-ICA 78

LIST OF SYMBOLS AND ABBREVIATIONS

Abbreviations used in this Thesis

FFT	Fast Fourier Transform
DFT	Discrete Fourier Transform
IMF	Intrinsic Mode Functions
ICA	Independent Component Analysis
FFT-En	Fast Fourier Transform and Envelope Analysis
SVM	Support Vector Machine
CWRU	Case Western Reserve University
EDM	Electro-Discharge Machining
PCA	Principal Component Analysis
KKT	Karush-Kuhn-Tucker

Symbols used in Section 3.1

$F(\omega)$, $f_{br}(t)$, and $f_{br}(t)$	The healthy motor, broken rotor bar motor and bearing-fault motor vibration signatures in frequency-domain
$f(t)$	The time-domain signature
t_i	The time point

$FFT()$	Fast Fourier transform function
Re x[ ], Im x[ ]	The real part, imagine part of time domain signal
N	The length of the signal
$a(\omega_i)$, $a_{br}(\omega_i)$, and $a_{be}(\omega_i)$	Magnitude information of healthy motor, broken rotor bar motor and bearing-fault motor
ω_i	Frequency components
$\Delta\omega$	The selected resolution
A_b, A_{br}, and A_{be}	Healthy, broken rotor bar fault, and bearing fault frequency characteristics of motors

Symbols used in Section 3.2

x(t)	narrow band signal at time *t*.
$\hat{x}(t)$	Hilbert transformation's mathematical description
f_0	Waveform frequency
$\Phi(t)$	The amount of phase modulation

Symbols used in Section 4.1

y_1, y_2	Random variables
$E\{\}$	Covariance function of variables
$P()$	Joint probability density function
λ	Maximum amplitude
x	Observed variable
x, $\hat{\mathbf{x}}$	Data vector

$\boldsymbol{X}$	n-dimensions measured signal vectors
$\boldsymbol{Y}$	Statistically independent components
$\boldsymbol{W}$	Transformation matrix
$J()$	Negentropy function
$G()$	non-quadratic function
v	Gaussian variable
$\boldsymbol{I}$	Identity matrix
$\boldsymbol{ICs}$	set of mutually independent vectors
$\boldsymbol{A}$	constant mixing matrix
$F_{signals}$	Signatures matrix
$a_m(\omega i)$	The magnitude information of component
ωi	Component of signature

Symbols used in Section 5.1

S	Training set
$\overline{S}$	Test set
Σ	All data sets
N	Number of training set
$\overline{N}$	Number of test set
d_i	The label of each sample
x_{i}	Each sample
$g(\boldsymbol{x})$	Discriminant function
$\boldsymbol{w}$, b	weights, bias

sgn []	Sign function
γ_i^f , γ_i^g	Function, geometric margin of an example
γ^f , γ^g	Function, geometric margin of a training set
α_i and β_i	Lagrange multipliers
$L()$	Lagrange function

CHAPTER 1

INTRODUCTION

1.1 Motivations and Objectives

Induction motors play a significant role as essential power in transportation, production and manufacturing industries due to their robust design, simplicity in construction and relatively low cost. The performance of induction motors is closely related to guarantee its health operational condition. Although the robustness and reliability of induction motors is relatively high, some unforeseen faults are unavoidable. If they are badly damaged, problems such as rotor bar failures, stator winding failures and bearing failure will occur. The unexpected failure of induction motors will lead to catastrophic consequences in marine vessel, transportation vehicles and other situations.

To achieve automatic diagnosis and detection aim, it is crucial to establish understanding of early fault diagnosis. Currently, main procedures of motors maintenance contain periodic visual inspections and replacement of damaged units at machine down time. Nevertheless, at the initial period of faults appearance, it is difficult to perceive motors faults at high speed rotation since failure degree is very slight. The faults can only be found when the motors make big noise or vibrate strongly. Early fault diagnosis and detection can reduce unscheduled machinery outages, consequential damage and maintenance cost. Therefore, it is important to develop a system to automatic fault detection continuously for improving motor performance and prolonging machine life.

A typical system of induction motor fault detection is illustrated as Fig. 1.1. The main parts of the system are data acquisition, data pre-processing, analysis algorithm, and data post-processing based on the results from algorithm. The signature from induction motor is collected using accelerometers or optical encoder. Data pre-processing and analyzing are post processed in a Matrix Laboratory or Digital Signal Processing environment. Finally, the system can automatically diagnose the condition of induction motor.

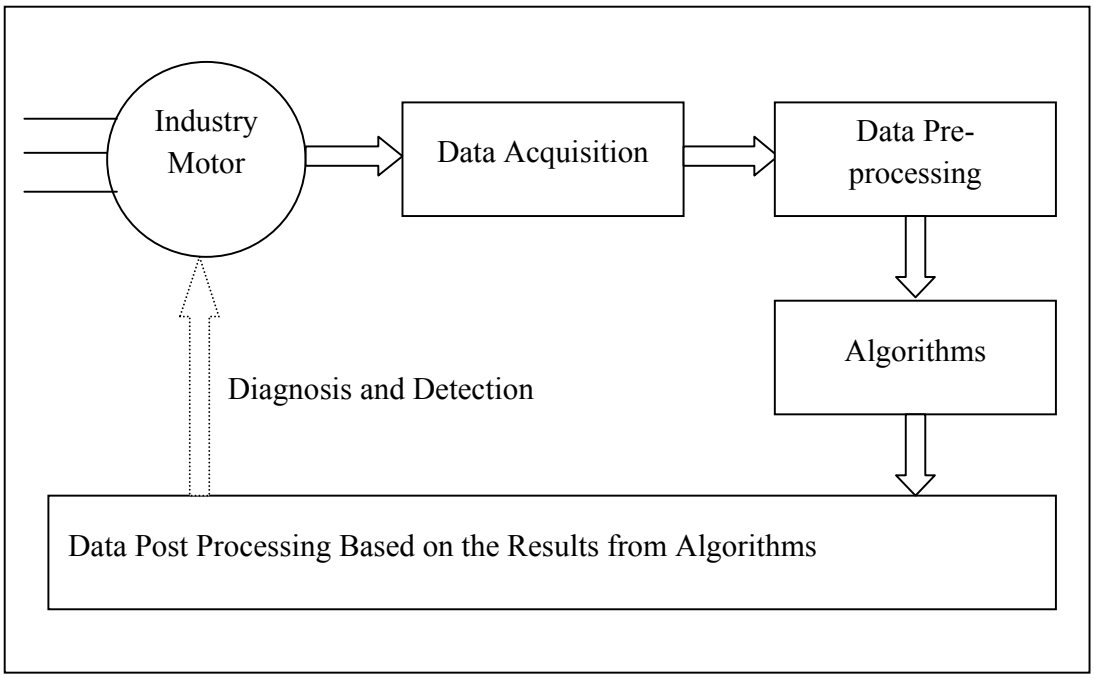

Fig. 1.1 A typical system of induction motor fault detection

Most motor fault signals are mixed in power frequency. Effective diagnosis and condition monitoring of an induction motor mechanical faults is not only important but complicated. Thus, the second aim of this thesis is to find a reasonable and effective way to process vibration signals.

1.2 Previous Work and Contributions of This Thesis

There is a significant amount of research in motors fault detection area. However vibration (acoustic) and current (electromagnetic flux) information are generally used for condition monitoring of induction motors. Even though current signal analysis is providing continuous monitoring in a nonintrusive way, vibration signal analysis is more commonly used for periodic inspections in industry. This thesis is based on spectra analysis of the vibration data.

Previous research developed varieties of methods to detect and diagnose motors fault on vibration signal, including the Fourier spectrum, wavelet package, the Kullback index of complexity, pseudo-phase diagrams, singular spectrum analysis, and fuzzy logic classification techniques, neural networks, etc [2]. These methods can be classified into time domain, frequency domain, time-frequency domain, higher-order spectra analysis, neural-network, and model-based techniques [3].

In the time domain, approaches enhance vibration signals through a filtering and direct analysis signals morphology or some other related time domain signal statistical parameters, such as peak, kurtosis and crest factor. This technique is simple, but it has crucial shortcoming. For instance, some approach detects fault by the values of kurtosis and crest factor, which can measure the spikiness of the vibration signal in the motors slight damage stage. However, when the motors degradation level increases, vibration signals become random, and kurtosis and crest factor lack the ability of measuring signal spikiness. Therefore, this thesis is based on analysis in the frequency domain instead of time domain.

Frequency domain analysis can also be named spectrum analysis. Vibrations signals are commonly converted from time domain to frequency domain by the Fourier transform. In the frequency domain, the signal information of time domain is converted to a magnitude and phase component of each frequency. The important purpose for vibration signals analysis of this thesis in the frequency domain is the analysis of signal properties. The vibration spectrum contains harmonics associated with the defective component of induction motor. As damage occur in a motor, the spectrum peaks at the corresponding motor defect frequency. Furthermore, there are sidebands around each peak. The spacing of the sidebands depends on the periodic properties of the loading and transmission path [4]. The vibration spectrum amplitudes of the peaks increase, as the corresponding motor component damage increases.

In the time and frequency domain, approaches utilize both time and frequency domain information to analysis signal transient features, including wavelet transform, short-time Fourier transform, etc.

High-order spectra show the corresponding phase angles among different signal frequencies. The bispectrum and trispectrum analysis are generally used to derive features, which are related to the motor condition.

Model-based techniques require to study and dependent on the system information. Mathematical models are built according to mechanical systems and reflect the relationship between the vibration signals received from specific location sensor and the type of fault present in the motor.

Neural networks are widely applied to signal processing in recently years, and some of which have the characteristic of self-organizing, self-learning and parallel processing of distributed information. To use this approach in motor detection and diagnose a feature extraction algorithm is needed to provide useful information to train the neural network. Since motor fault detection and diagnosis is first of all a pattern recognition problem. This algorithm strongly determines the performance of neural networks approach. This thesis using ICA extracts signal features from the vibration data, and then uses these features to train and test neural networks. These features then are classified into the required number of healthy and faulty clusters in the feature space, which are then used to measure the health condition of the induction motor.

In view of that the above, this thesis proposes an easy-to-implement and efficient system to detect and diagnose status of induction motors and electromechanical systems by providing vibration signature analysis in the frequency-domain. This system combines Fast-Fourier-Transform technology with Envelope Analysis, which is widely known as the high frequency resonance technique, greatly reduces the noise influence and more effectively extracts fault signals. This system also proposes an automatic and effective design for signals classification. It applies ICA, extracts features obtained from the results of FFT-En, and then uses SVM separate these features from each other in the feature space. Therefore, this thesis explores an automatic way to monitor and diagnosis induction motors and electromechanical systems instead of manual diagnosis, and achieves a diagnostic accuracy of almost 100%.

1.3 Thesis Outline

This thesis aims to develop an automatic software platform for fault detection and diagnosis of induction motors and electromechanical systems, analyzing vibration data features and studying and comparing related algorithm, and targeting at a robust and highly accurate fault classification. In addition to fault detection on induction motors, the platform has also been applied to fault detection on wind-power turbines and train-drive system of Singapore's mass-rapid transit railway to demonstrate its robustness for detecting abnormal vibrations in complex electromechanical systems. As shown in Fig. 1.2, the platform uses FFT and Envelope Analysis for processing each time-domain healthy or faulty waveform collected from a healthy or faulty motor, ICA for extracting the features to describe its signature as identified by Envelope Analysis and SVM for classifying between healthy and faulty signatures. The in-depth description of each component of the proposed platform will be given in remaining Chapters of this thesis.

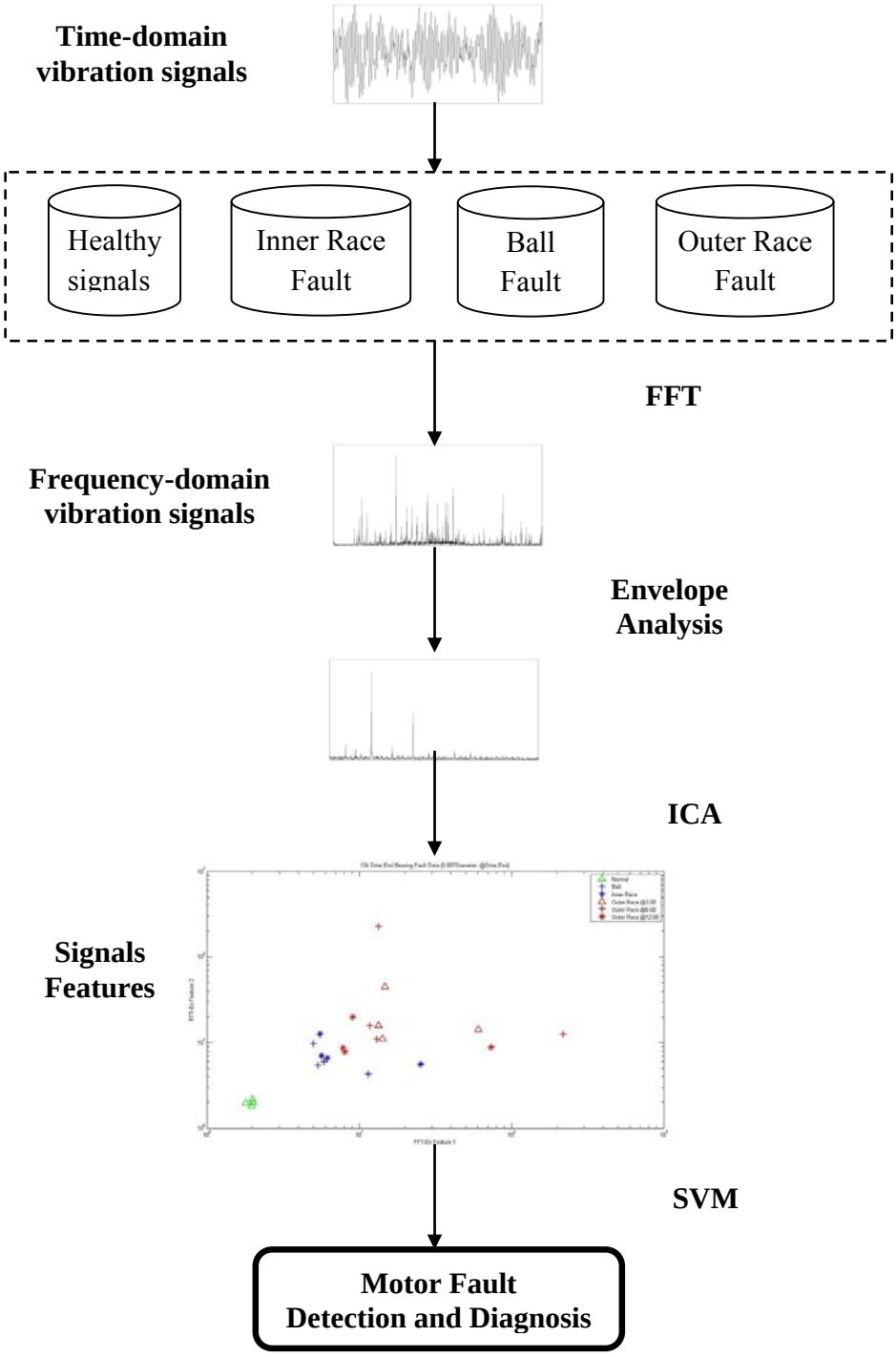

Fig. 1.2 Proposed automatic motor fault detection and diagnosis scheme

The thesis is therefore organized as follows:

Chapter 1 introduces the motivations and objectives of this thesis, reviews earlier work, summarizes the contributions of this research, and shows the thesis outline.

Chapter 2 focuses on the structure and operation principle of induction motor, and introduces the classification of induction motor faults. This thesis mainly studies the detection and diagnosis of bearing fault, and additional source of vibration data sets are from three different research organizations outside NUS: Bearing Data Center of Case Western Reserve University, Vestas R&D Centre (Singapore) and SKF.

Chapter 3 describes the definition and principle of FFT-Envelope Analysis, which is used to extract the feature of vibration signature of induction motors and electromechanical systems. This system uses Fast Fourier Transformation to transform the signal from time domain to frequency domain, and then uses Envelope Analysis to reduce the noise influence and extract the fault signals. In the last Section of this Chapter, it presents three groups of results by using FFT-En.

Chapter 4 focuses on the principle and implementation of Independent Component Analysis (ICA). Due to the simple and reliability of ICA, this thesis adopts it as a feature extraction method in induction machine condition monitoring and fault diagnosis field. Furthermore, demonstrations on how FastICA works are presented at the end of this Chapter.

The application of neural networks is widely employed to solve classification problem for condition monitoring and fault diagnosis. Chapter 5 introduces a machine-learning

algorithm SVM and how it is applied in the case of induction motors and electromechanical systems condition detection.

Chapter 6 presents and discusses results of the proposed method of condition detection and diagnosis of induction motors and electromechanical systems.

Chapter 7 concludes the present research completed with automatic detection and high accuracy and proposes the future work by development of a more powerful SVM and more efficient Zoom-FFT into the system for more types of induction motors and electromechanical systems faults detection.

CHAPTER 2

INDUCTION MOTOR AND DATA COLLECTION

2.1 Introduction

2.1.1 Structure of Induction Motor

Induction motors are widely used in industrial drives, because they have the characteristics of practicality, robustness, simplicity in construction, and relatively low capital/maintenance costs. Their speed is determined by the supply or inverter frequency.

A labeled cutaway view of a typical motor is demonstrated in the Fig. 2.1.1-a) [5] below, which shows the main parts: the stator, rotor, and enclosure.

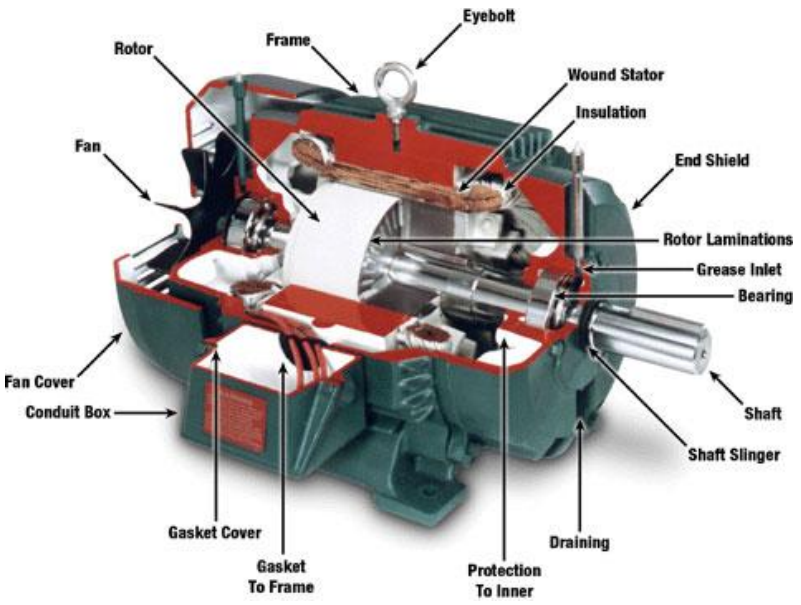

Fig. 2.1.1-a) Structure of an induction motor [5]

The stator is the motor's outside stationary part, which is illustrated in Fig. 2.1.1-b) [6]. Many thin metal sheets, called laminations, are made as stator core to keep down energy loses. Laminations are normally made by steel and form a hollow cylinder. Coils of insulated wire placed in slots of the motor housing, and the stator windings are directly linked to the power source. When the current is supplied, coils become electromagnets. Electromagnetism is the essential principle of the motor operation.

Fig. 2.1.1-b) The stator of an induction motor [6]

The rotor is the inside rotating part of the motor's electromagnetic circuit. Fig. 2.1.1-c) [6] provides the cutaway view of motor rotor. The most common type of rotor used in asynchronous motor is the "squirrel cage" rotor, which consists of evenly spaced conductor bars around the cylinder of the end rings covered by stacking thin steel laminations to reduce eddy current. After die casting, rotor conductor bars are mechanically and electrically connected with end rings. Then, the rotor is pressed onto a shaft to form an integral part of the rotor construction.

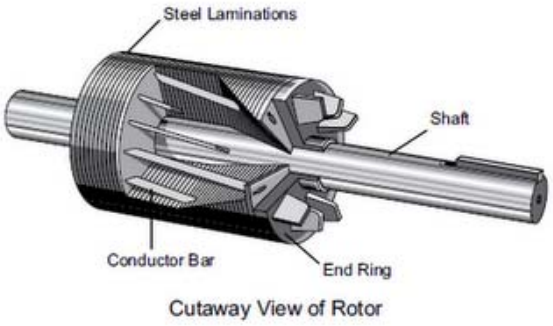

Fig. 2.1.1-c) The rotor of an induction motor [6]

The enclosure consists of a frame and two bearing housings. As shown in Fig. 2.1.1-d) [6], the rotor is inside the stator, which is assembled in the motor frame. There is an air gap to provide no direct physical connection between the rotor and stator. Bearings are mounted on the shaft to support the rotor.

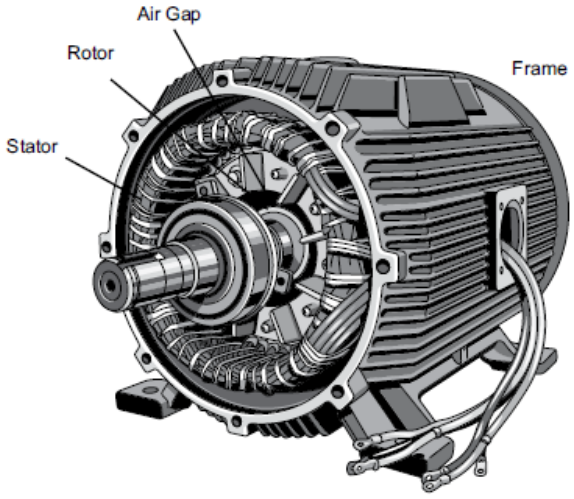

Fig. 2.1.1-d) Partially assembled motor [6]

2.1.2 Basic Operation of Induction Motor

Insulated wire coils are placed in stator slots of motors. The principle of rotating magnetic field explains the shaft rotation of motors. Fig. 2.1.2-a) [7] shows a schematic diagram of three-phase stator.

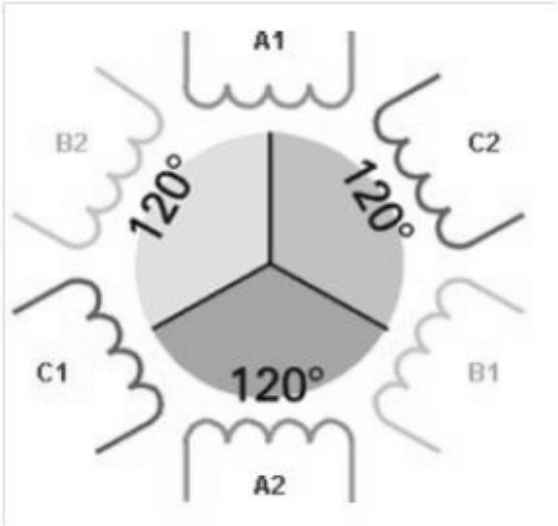

Fig. 2.1.2-a) A 3-phase stator [7]

In this example, three-phase windings (A, B, and C) are separated by 120° from one another, and a second set of three-phase windings is placed between the space. This is a 2 poles stator. Because each phase winding appears twice, the number of times that a phase winding appears determines the number of poles.

When the stator is connected to a 3-phase AC power supply, current flows through the windings. The direction of the current flow through winding decides the magnetic pole of the phase winding. Fig. 2.1.2-b) [7] illustrates how three-phase power

produces a rotating magnetic field. In this example, we assume that A1, B1 and C1 windings connect to a positive current and result in a north pole.

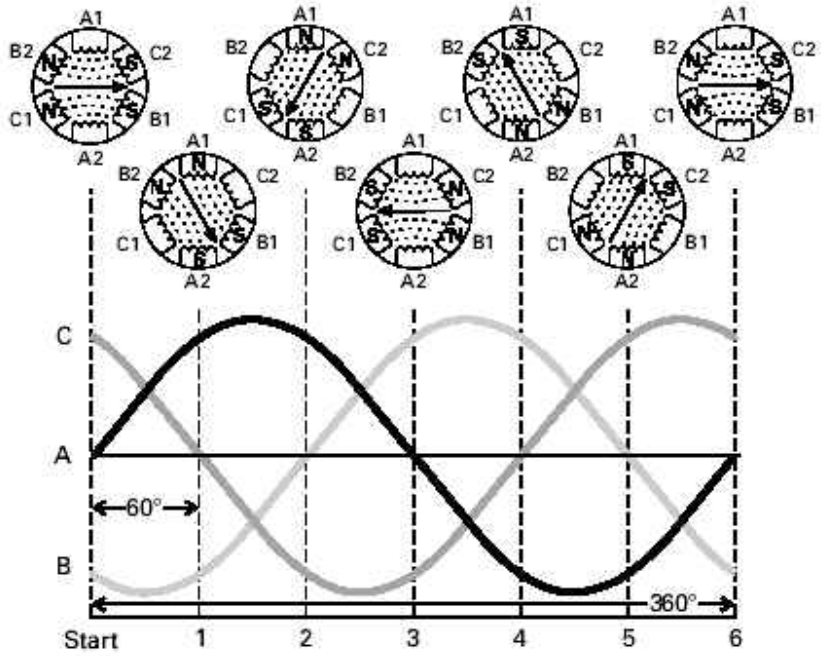

Fig. 2.1.2-b) 360 degree rotation [7]

At time instant 0, phase A has no current flow, phase B has a negative current flow, and phase C has a positive current flow. Furthermore, windings B_2 and C_1 become north poles, windings B_1 and C_2 become south poles, and a magnetic field results, which direction as the arrow in the illustration.

At time instant 1 (angle = 60°), phase C has no current flow, phase A has a positive current flow, and phase B has a negative current flow. Similarly, windings A_1 and B_2 become north poles, windings A_2 and B_1 become south poles, and the magnetic field has rotated 60°.

At time instant 2, phase A has a decreasing positive current flow, phase B has no current flow, and phase C has a negative direction. Thus, windings A_1 and C_2 become north poles, windings C_1 and A_2 become south poles, and the magnetic field has rotated 60°.

Therefore, the magnetic field will rotate 360 degree (a full revolution) at the end of time instant 6. Such fields will vary 50 times per second on a 50 Hz power supply.

2.2 Fault Specifications

There are two types of induction motor faults studied in the thesis: mechanical faults, which include bearing faults, gear faults, mechanical looseness, etc., and electrical faults, which include unbalanced power supply, non-even air-gap, imbalance in motor load, stator-winding, etc.

Fig. 2.2 Fault located on the bearing

A bearing is the machine element that supports the rotor bar. Fig. 2.2 indicates a bearing-fault that was created on a motor with a dent on the seal connected to the inner

race of the bearing. According to the investigation carried out by the Electric Power Research Institute, the most common failure faults in induction motor is failure of rolling element bearing followed by stator winding failures and rotor bar failures. A bearing failure will increase the rotor rotational friction, reduce the efficiency of induction motors, and cause overheating and to wear to the motor. Therefore, diagnosing bearing health is extremely important for the reliability of induction motor systems. In this thesis, bearing-fault detection and diagnosis will be studied.

2.3 Data Collection

This thesis studies three groups of vibration data, from the Bearing Data Center of Case Western Reserve University (CWRU) [8], Vestas R&D Centre in Singapore and Svenska Kullager-Fabriken in Singapore (SKF) respectively.

2.3.1 Data from CWRU [8]

There are 4 sets of data from CWRU, which collected the vibration data for normal and faulty bearings using a 2 hp Reliance Electric motor. Motor bearings faults were made by electro-discharge machining (EDM), and their diameter is 0.007-0.040 inches located at the bearing ball, inner raceway, or outer raceway. The information of motor bearing used in simulation is shown in Table 2.3.1-a) [8].

Table 2.3.1-a) Defect frequencies: (multiple of running speed in Hz) [8]

Type	Inner Ring	Outer Ring	Cage Train	Rolling Element
Drive-end	5.4152	3.5848	0.39828	4.7135
Fan-end	4.9469	3.0530	0.3817	3.9874

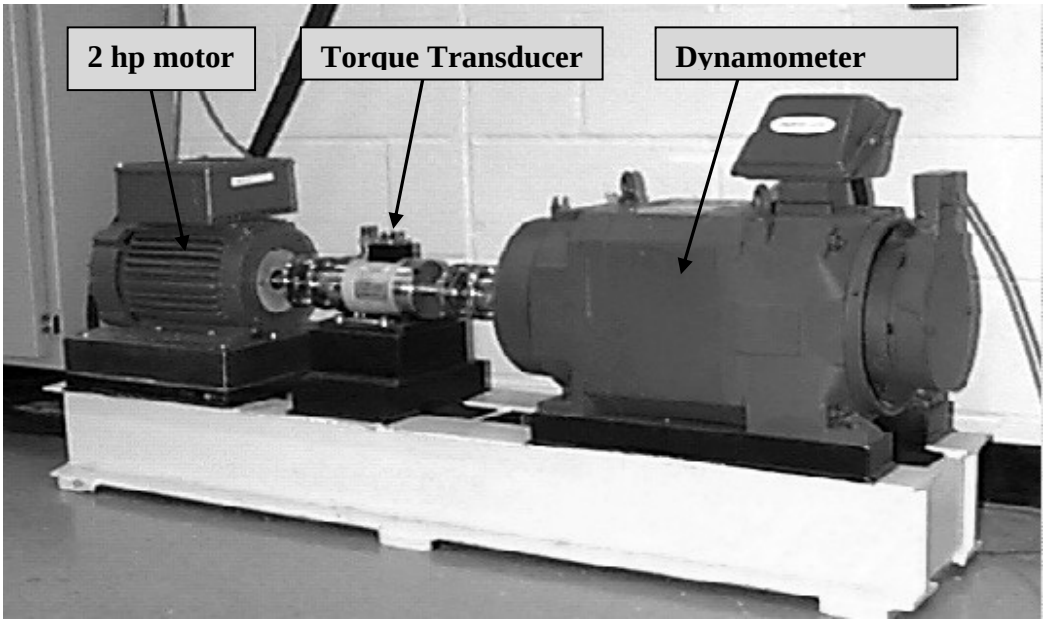

Fig. 2.3.1 Test stand [8]

As shown in Fig. 2.3.1 [8] above, the test stand supports a dynamometer, a torque transducer, a 2 hp motor and control electronics, which are not shown in this figure.

The test motor bearings faults were drilled by EDM. The fault diameters on SKF bearing are 0.007 inches, 0.014 inches, and 0.021 inches, and the fault diameters on NTN bearing are 0.028 inches, and 0.040 inches. Table A.2.3.1-b) [8] and Table 2.3.1-c) [8] provide the diameter and depth information of holes to simulate different bearing fault.

Table 2.3.1-b) Drive-end bearing-fault specifications (1 mil=0.001 inches) [8]

Location	Inner Raceway				Outer Raceway				Ball			
Diameter	7	14	21	28	7	14	21	40	7	14	21	28
Depth	11	11	11	50	11	11	11	50	11	11	11	150
Type	SKF	SKF	SKF	NTN	SKF	SKF	SKF	NTN	SKF	SKF	SKF	NTN

Table 2.3.1-c) Fan-end bearing-fault specifications (1 mil=0.001 inches) [8]

Location	Inner Raceway			Outer Raceway			Ball		
Diameter	7	14	21	7	14	21	7	14	21
Depth	11	11	11	11	11	11	11	11	11
Type	SKF	SKF	SKF	SKF	SKF	SKF	SKF	SKF	SKF

Vibration data pre-processed in a MATLAB platform are recorded in .mat format at 12,000 samples/second for drive and fan-end bearing faults, and at 48,000 samples/second only for drive-end bearing faults.

The data was collected by vibration sensors, which were placed with magnetic bases at the 12 o'clock position at both of the motor drive-end and fan-end. The data of motor speed (from 1797 to 1720 RPM) and motor loads (from 0 to 3 horsepower) were collected by torque transducer and recorded manually. Table 2.3.1-d) [8] indicates the collection speed and load of normal baseline data.

Table 2.3.1-d) Normal baseline data [8]

Motor Load (HP)	Approx. Motor Speed (rpm)	Normal Baseline Data
0	1797	Normal_0
1	1772	Normal_1
2	1750	Normal_2
3	1730	Normal_3

Outer raceway is stationary. Therefore, the placement of the fault directly affects motor vibration response. In order to quantify this effect, the experiments for bearing

outer raceway faults (including fan and drive-end bearing) placed vibration sensors at three different places: load zone (3 o'clock), load orthogonal zone (6 o'clock), and 12 o'clock. Collection information of fault bearing data is listed in the appendix A.1 CWRU Vibration data Information.

2.3.2 Data from Vestas

There are 18 sets of data from Vestas, which collected the wind-power generator bearing vibration data using accelerometers. Accelerometers were placed on three turbines and at Generator Drive-end and not Generator Drive-end for each turbine. And the data were recorded in different time period and the recording time for each is around 40 seconds. The detail of collection date and time is shown in Table 2.3.2.

Table 2.3.2 Vestas in Singapore vibration data record list

Turbines	Accelerometers Location	Collection Date and Time		
No.10	GDE	26-Mar-2009 18.00.05	25-Oct-2008 01.31.50	16-Sep-2008 16.12.31
	GNDE	26-Mar-2009 18.00.05	25-Oct-2008 01.31.50	16-Sep-2008 16.12.31
No.31	GDE	17-Apr-2009 05.59.30	27-Jun-2009 08.12.46	19-Mar-2009 12.23.36
	GNDE	17-Apr-2009 05.59.30	27-Jun-2009 08.12.46	19-Mar-2009 12.23.36
No.44	GDE	24-Dec-2007 05.21.22	24-Dec-2007 13.18.18	22-Feb-2008 23.49.03
	GNDE	15-Oct-2007	24-Dec-2007	24-Dec-2007

		16.29.34	05.21.22	13.18.18

(GDE means Generator Drive-end, GNDE means not Generator Drive-end)

2.3.3 Data from SKF

There are 2 sets of vibration data from SKF, which collected on two different motors (Motor AHU 124 and Motor RCU 01). For Motor AHU 124 sampling frequency is 2560 Hz and number of samples is 2048, and for Motor RCU 01 sampling frequency is 1280 Hz and number of samples is 2048.

CHAPTER 3

SIGNATURE FEATURE EXTRACTION

3.1 Theoretical Analysis of the Proposed FFT

Fourier Transform is an important algorithm in the fault detection field. According to Fourier principle, a continuous measurement of the timing or signal can be represented by infinite superposition of different frequency sine wave signals. On this principle, Fourier transform cumulatively calculates the frequency, amplitude and phase of sine wave signals in the original signal by using direct measurements. Inverse Fourier transform is essentially also a treatment of cumulative, which can convert independent sine wave signals into a new signal. Therefore, Fourier transform can convert original time-domain signal, which is difficult to deal, into a new frequency-domain signal, which is easy to process and analysis by tools.

FFT, which is a fast algorithm for the discrete Fourier transform, can transform a signal into the frequency domain. This signal in time-domain is difficult to see its features, but it is easier to analyze the features transformation in frequency-domain.

From the view of modern mathematics, the Fourier transform is a special integral transformation. The frequency-domain signal *F(ω)* can be transformed from an original time-domain signal *f(t)* by using FFT [9]:

$$f(t) \rightarrow (f(t_1)f(t_2) \dots f(t_L)) \tag{3.1.1}$$

Here $f(t_i)(i = 1,2, \dots, L)$ is amplitude, and $t_i(i = 1,2, \dots, L)$ means time point, where L records the number of samples.

$$F(\omega) = FFT(f(t)) \tag{3.1.2}$$

where *FFT* represents fast Fourier transform function.

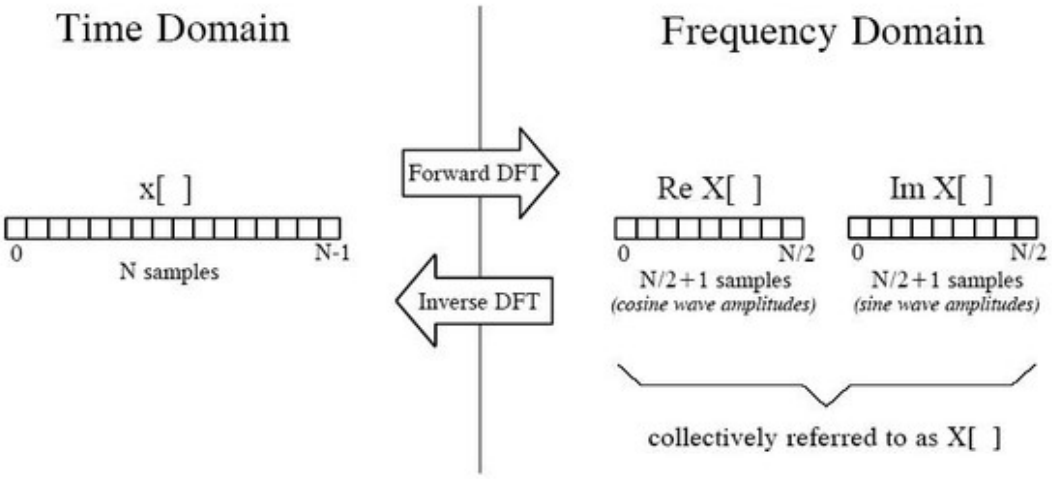

Fig. 3.1 The process of DFT and Inverse DFT

Fig. 3.1 [10] indicates the method of transformation signals from time-domain to frequency-domain and the inverse process. The left part of illustration represents signals in time-domain, and the right part represents signals in frequency –domain.

where x[ ] is the time domain signal, and N is the length of this signal;

Re x[ ] and Im x[ ] represent real part and imagine part of frequency domain, respectively. N/2+1 is the length of these signals.

The MATLAB source code of FFT arithmetic used in this system is attached in the Appendix 2.1.

$$F(\omega) \rightarrow (a(\omega_1)\, a(\omega_2)\ \ldots\ a(\omega_N)) \tag{3.1.3}$$

Here $a(\omega_i)(i = 1,2,\ldots,N)$ represents the magnitude information, where N is the selected number of the frequency components $\omega_i(i = 1,2,\ldots,N)$, and $\Delta\omega = \omega_{i+1} - \omega_i$ is the selected resolution.

The frequency-domain signal $F(\omega)$ generated by transformation (3.1.2) includes the magnitude information about each frequency components as the above (3.1.3)

$$F_{br}(\omega) \rightarrow (a_{br}(\omega_1)\, a_{br}(\omega_2)\ \ldots\ a_{br}(\omega_N)) \tag{3.1.4}$$

$$F_{be}(\omega) \rightarrow (a_{be}(\omega_1)\, a_{be}(\omega_2)\ \ldots\ a_{be}(\omega_N)) \tag{3.1.5}$$

where $F(\omega)$, $f_{br}(t)$, and $f_{br}(t)$ represent the healthy motor, broken rotor bar motor and bearing-fault motor vibration signatures in frequency-domain, respectively.

$a_{br}(\omega_i)(i = 1,2,\ldots,N)$ and $a_{be}(\omega_i)(i = 1,2,\ldots,N)$ represents the magnitudes of two kinds of faulty motors, where N is the number of the frequency components $\omega_i(i = 1,2,\ldots,N)$.

The frequency spectrum of the bearing-fault motor has the frequency signatures of the bearing faults around the fundamental harmonics, and the frequency spectrum of the broken rotor-bar motor has sidebands around the fundamental harmonics. Therefore, (3.1.3), (3.1.4) and (3.1.5) can be merged into (3.1.6) in the following.

$$F\_signals=$$

$$\begin{pmatrix} a(\omega_1)\, a(\omega_2) \ldots a(\omega_n) & \overbrace{0 \ldots 0}^{k} & \overbrace{0 \ldots 0}^{m} \\ a(\omega_1)\, a(\omega_2) \ldots a(\omega_n) & a(\omega_{br1})\, a(\omega_{br2}) \ldots a(\omega_{brk}) & \overbrace{0 \ldots 0}^{m} \\ a(\omega_1)\, a(\omega_2) \ldots a(\omega_n) & \overbrace{0 \ldots 0}^{k} & a(\omega_{be1})\, a(\omega_{be2}) \ldots a(\omega_{bem}) \end{pmatrix}$$

(3.1.6)

Equation (3.1.6) can also be simplified as:

$$F\_signals = \begin{pmatrix} A_b & 0 & 0 \\ A_b & A_{br} & 0 \\ A_b & 0 & A_{be} \end{pmatrix} \quad (3.1.7)$$

Here $A_b\ equals\ (a(\omega_1)a(\omega_2) \ldots\ a(\omega_n))$, and represents the healthy frequency characteristics of motors.

$A_{br}\ equals\ (a(\omega_{br1})a(\omega_{br2}) \ldots\ a(\omega_{brk}))$, and represents the frequency characteristics of motors with broken rotor bar fault.

$A_{be}\ equals\ (a(\omega_{be1})a(\omega_{be2}) \ldots\ a(\omega_{bem}))$, and represents the frequency characteristics of motors with bearing fault.

In the first row of (3.1.7), there are magnitudes of healthy motor frequency components. The healthy motor is assumed to be perfectly normal, so the magnitudes of broken rotor bar and bearing faulty frequency components equal zero. In the same way, the second row of (3.1.7) represents the magnitudes of frequency signatures of broken rotor bar motor, and the magnitudes of bearing-fault frequency components equal zero.

Similarly, the third row of (3.1.7) shows the magnitudes of frequency signatures of bearing-fault motor, and the magnitudes of broken rotor bar fault frequency components equal zero.

From (3.1.7), it can be observed that healthy and different faults signatures have their own frequency characteristics, such as A_b, A_{br} and A_{be}. It means that healthy and faulty motors can be distinguished by the magnitudes of the frequency components rather than the frequency components themselves. For example, if the frequency components are fundamental constants, the system can diagnose motors healthy status and faults type only by the magnitudes of the frequency components and regardless of other motor parameters.

Therefore, this Section proposes a frequency-domain signals analysis algorithm using the magnitudes of the selected frequency components. The benefit of this algorithm is that the detection process does not need the information of the frequency spectrum range, which is based on the inverter frequency and must be estimated for new set of signals.

3.2 Envelope Analysis

Envelope Analysis, which can extract the related characteristics of signals from high frequency modulation signatures, is generally used as frequency analysis technique for the detection and diagnosis of induction motors and electromechanical systems faults.

The principle of signatures analysis of Envelope Analysis is using wavelet analysis to find fault signal band and envelope spectrum analysis in the signal band by Hilbert transformation.

3.2.1 Steps of the Envelope Analysis

Envelope Analysis is signatures demodulation method as theoretically based on the Hilbert transformation. The major steps are showed in Fig. 3.2.1.

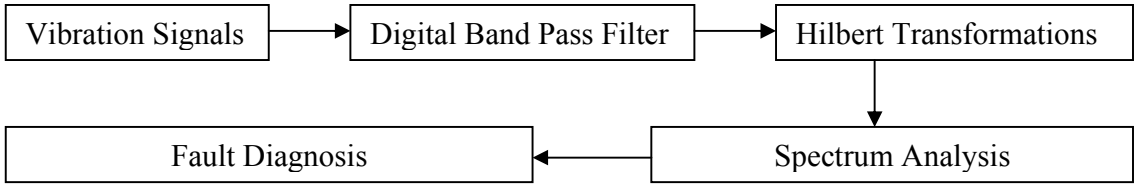

Fig. 3.2.1 Steps of Envelope Analysis diagnosis

Firstly, Envelope Analysis, which is the high frequency resonance method, extracts the resonance frequency band of the natural frequency of fault signal using wavelet packet transform filtering, and reconstructs this signal to filter out the interference of other signatures frequency component. Then, Envelope Analysis implements envelope demodulation by using Hilbert transform to extract the reconstructed signal, removes high frequency natural vibration components, and finally finds the fault band and diagnoses defect information of fault induction motors and electromechanical systems.

3.2.2 Definition of Hilbert Transformation

Theory of Hilbert Envelope Analysis is the envelope of the absolute value of signatures, extract modulated signals, and analyze the changes of the modulation function, which greatly advantage extraction of fault characteristic.

The function of Hilbert transformation is made the phase of all frequency components of raw signature waveform shift -90 degree. Equation (3.2.2.1) and (3.2.2.2) [11] indicate

the mathematical description of Hilbert transformation in time-domain. Mathematical description of Hilbert transformation in frequency-domain is provided in (3.2.2.3) [11].

$$\hat{x}(t) = \frac{1}{\pi}\int_{-\infty}^{\infty} \frac{x(\tau)}{t-\tau} d\tau == \frac{1}{\pi}\int_{-\infty}^{\infty} \frac{x(t-\tau)}{\tau} d\tau = x(t) * \frac{1}{\pi t} \quad (3.2.2.1)$$

$$x(t) = \frac{1}{\pi}\int_{-\infty}^{\infty} \frac{\hat{x}(\tau)}{t-\tau} d\tau \quad (3.2.2.2)$$

$$\hat{x} = -j\, sgn(\omega) X(\omega) \quad (3.2.2.3)$$

3.2.3 Demodulation Principle of Hilbert Transformation

Hilbert Envelope Analysis, which isolates low-frequency information from raw signatures, has demodulation functions. It can obtain the envelope spectrum by analyzing spectra of the envelope signatures. In Hilbert-Huang transformation, a real signature is expressed as complex/ analytic signatures. The results consist of Envelope Analysis, instantaneous frequency and instantaneous phase of the real signature. Therefore, the results obtained by Envelope Analysis are generally clearer and more effective.

Equation (3.2.3.1) presents the real signature. Equation (3.2.3.2) is the analytic signature of this signal.

$$x(t) = A(t)\cos[2\pi f_0 t + \Phi(t)] \quad (3.2.3.1)$$

where *x(t)* is narrow band signal at time *t*.

$$z(t) = x(t) + \hat{x}(t) = A(t)e^{j[2\pi f_0 t + \Phi(t)]} \quad (3.2.3.2)$$

When *x(t)* is phase-modulated signature, *z(t)* can be expressed as in (3.2.3.3):

$$z(t) = |z(t)|e^{j[2\pi f_0 t + \Phi(t)]} = A(t)e^{j[2\pi f_0 t + \Phi(t)]} \quad (3.2.3.3)$$

where f_0 represents selected waveform frequency, and $\Phi(t)$ represents the amount of phase modulation. $\Phi(t)$ is given in (3.2.3.4),

$$\Phi(t) = \theta(t) - 2\pi f_0 t \quad (3.2.3.4)$$

Frequency modulation can be obtained from the differentiating of phase modulation, so the frequency modulated signal of the real signature $x(t)$ can be calculated by:

$$f(t) = d\Phi(t)/dt = d\theta(t)/dt - 2\pi f_0 \quad (3.2.3.5)$$

Therefore, the phase and frequency modulation data of the fault motor signals can be extracted by FFT and Envelope Analysis (FFT-En). The MATLAB source code of Envelope Analysis arithmetic used in this system is attached in the Appendix 2.2.

3.3 Vibration Data Processing

This thesis extracts feature from vibration induction motor signatures by using FFT-En. FFT transforms the raw waveform from time domain to frequency domain, then Envelope Analysis greatly reduces the noise influence and can more effectively extract the fault feature from the signature obtained through FFT.

This Section demonstrates a small part of data results, which are processed by FFT-En. More results of this system will be presented and discussed in Chapter 6.

3.3.1 Data Processing for CWRU [8]

There are 4 sets of data collected from CWRU, including one set of normal baseline data and 3 sets of bearing-fault data, and each set includes three types of bearing fault: ball-fault, inner race fault, and outer race fault.

The Top figure of Fig. 3.3.1-a) shows a raw vibration signal of normal bearing in the time-domain, the Middle figure is the plot of the signal transformed into frequency-domain using FFT, and the Bottom figure of Fig. 3.3.1-a) presents the feature of normal bearing signal processed by FFT and Envelope Analysis.

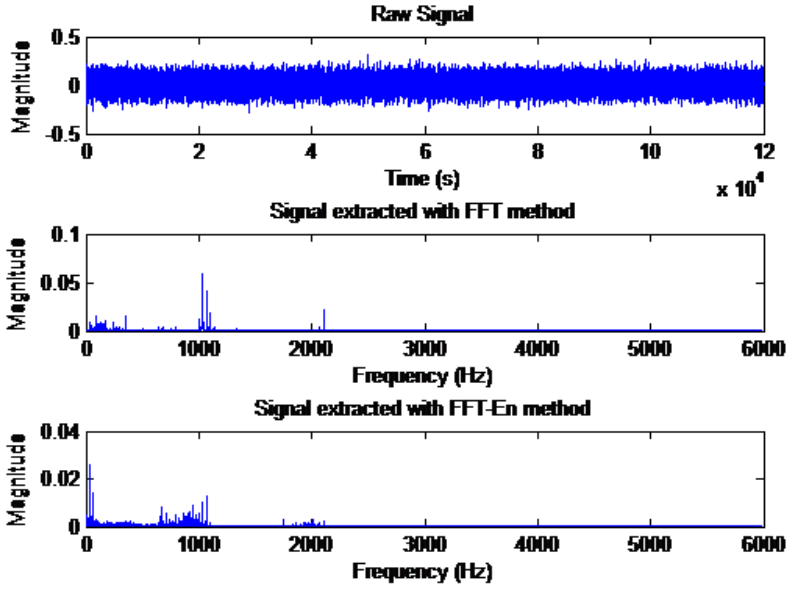

Fig. 3.3.1-a) FFT-En plot of normal bearing

The Top figure of Fig. 3.3.1-b) shows a raw vibration signal of drive-end bearing with ball-fault in time-domain, the Middle figure is the plot of the signal transformed into the

frequency-domain by FFT, and the Bottom presents the feature of ball-fault bearing signal processed by FFT and Envelope Analysis.

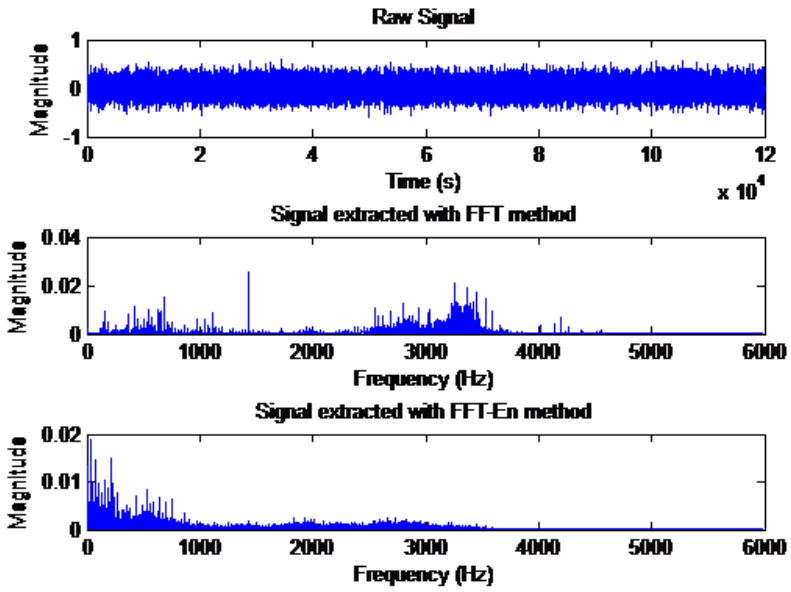

Fig. 3.3.1-b) FFT-En plot of ball—fault bearing

The data sets of Fig. 3.3.1-c-f) are collected from the same bearing as Fig. 3.3.1-b), however these bearings have race fault instead of ball-fault. Fig. 3.3.1-c) has inner race fault. Fig. 3.3.1 d-f) have the same outer race fault, but they are measured by three different vibration sensors, which placed at 3 o'clock, 6 o'clock, and 12 o'clock, respectively.

The Top plot of these four figures shows a raw vibration signal of race fault bearing in time-domain, the Middle figure is the plot of the signal transformed into frequency-domain using FFT, and the Bottom plot presents the feature of race fault bearing signal processed by FFT and Envelope Analysis.

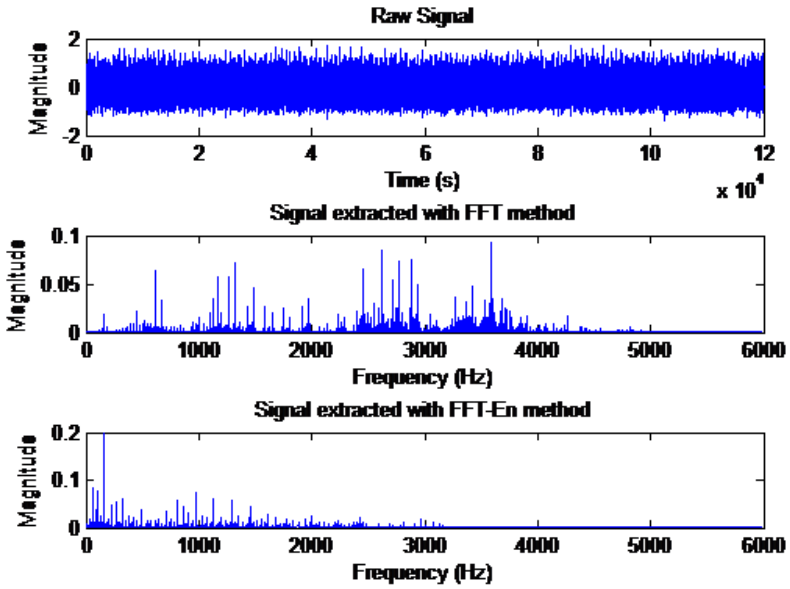

Fig. 3.3.1-c) FFT-En plot of inner race fault Bearing

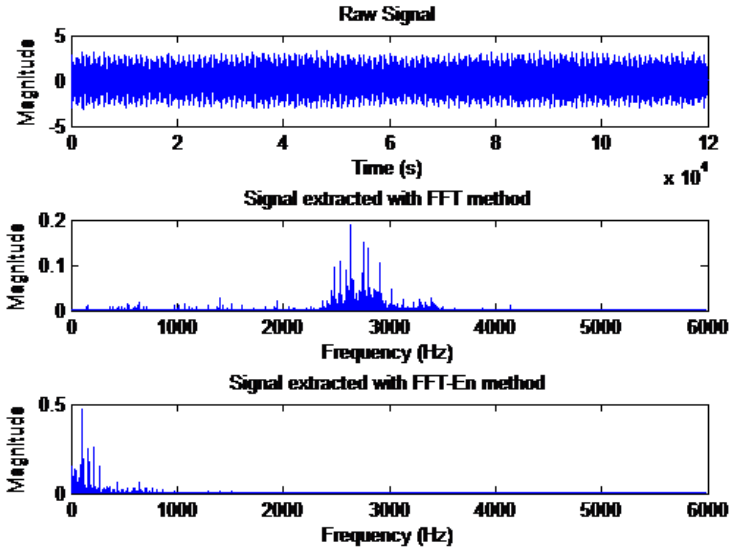

Fig. 3.3.1-d) FFT-En plot of outer race fault bearing @3 o'clock

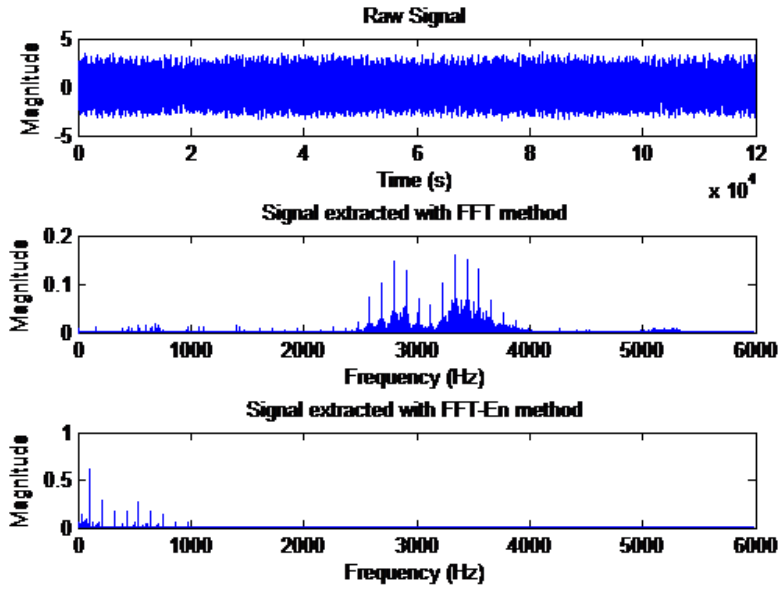

Fig. 3.3.1-e) FFT-En plot of outer race fault bearing @6 o'clock

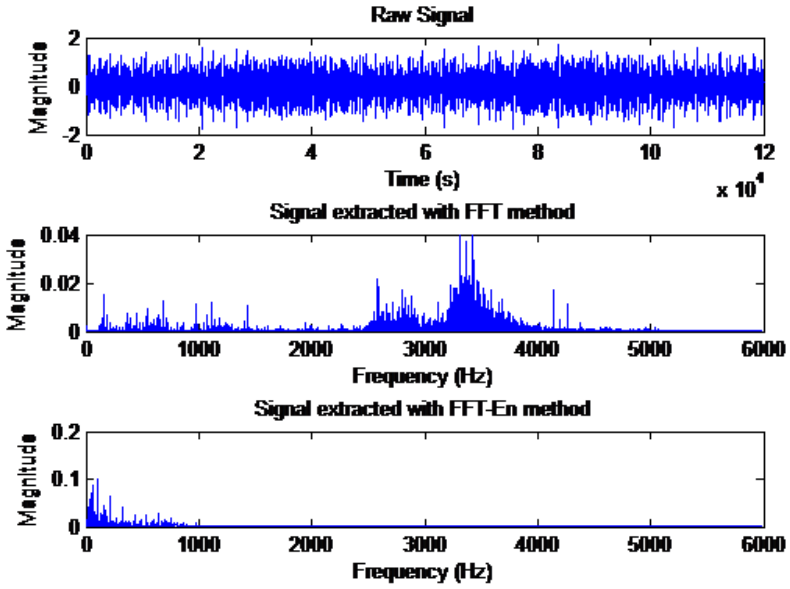

Fig. 3.3.1-f) FFT-En plot of outer race fault bearing @12 o'clock

From above figures, it can be concluded that healthy bearing and different type fault bearing from same motor have individual features. Furthermore, the features of Fig. 3.3.1-d), Fig. 3.3.1-e) and Fig. 3.3.1-f) are similar, because they all collected from the same bearing with the same type of bearing fault with vibration sensors placed at different locations.

Therefore, these results provide the basis for classifying different bearing faults. Furthermore, ICA will be used and that will be discussed in next Chapter, to classify these features and diagnose the status of motor/ bearing automatically.

3.3.2 Data Processing for Vestas

Eighteen sets of data were collected from Vestas's three different wind turbines (one turbine has bearing failure and the other two in good conditions).

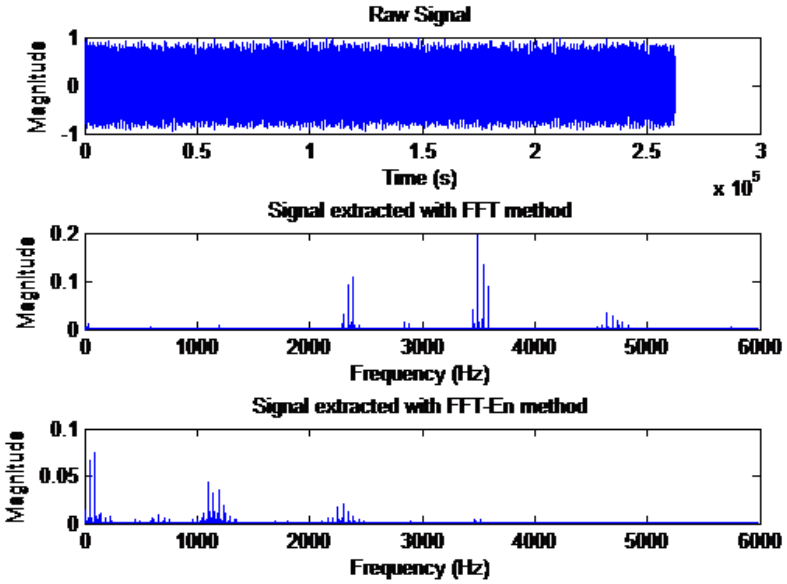

Fig. 3.3.2-a) FFT-En plot of a broken Vestas wind turbine

The Top figure of above Fig. 3.3.2-a) shows a raw vibration signal of faulty bearing located at generator drive-end of wind turbine No. 31, the Middle figure is the plot of the signal transformed from time-domain into frequency-domain using FFT, and the Bottom figure presents the feature of faulty bearing, which signal processed by FFT and Envelope Analysis.

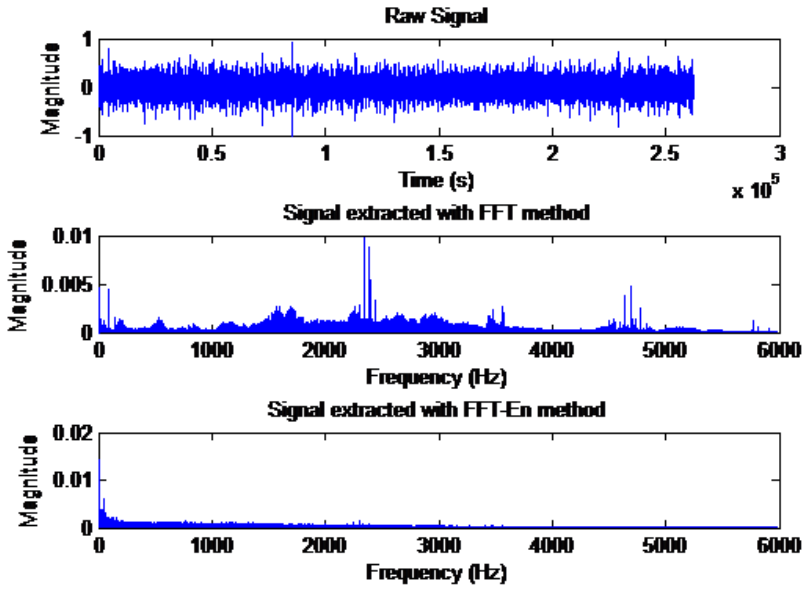

Fig. 3.3.2-b) FFT-En plot of a health Vestas wind turbine

The Top figure of above Fig. 3.3.2-b) shows a raw vibration signal of healthy bearing located at not generator drive-end of wind turbine No. 44, the Middle figure is the plot of the signal transformed from time-domain into frequency-domain using FFT, and the Bottom figure presents the feature of healthy bearing, which signal processed by FFT and Envelope Analysis.

From these two figures, it can be demonstrated that wind turbines with healthy bearing and faulty bearing have different features. Therefore, the status of wind turbine can be diagnosed by these features as further illustrated in Chapter 4.

3.3.3 Data Processing for SKF Data Sets

Two sets of data were collected from the same induction motor with two different SKF bearings.

The Top figure of Fig. 3.3.3-a) shows a raw vibration signal from the motor RCU01 with a healthy bearing in the time-domain, the Middle figure is the plot of the signal transformed into frequency-domain using FFT, and the Bottom figure presents the feature of this healthy motor signal processed by FFT and Envelope Analysis.

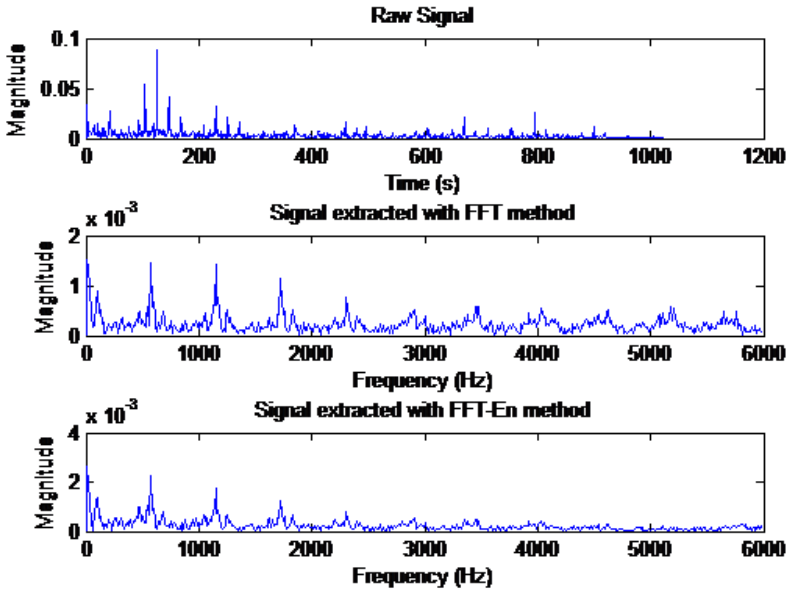

Fig. 3.3.3-a) FFT-En plot of a health motor SKF Bearing

The above figure of Fig. 3.3.3-b) shows a raw vibration signal of broken bearing RCU01, the Middle figure is the plot of the signal transformed from time-domain to frequency-domain using FFT, and the Bottom figure presents the feature of this broken motor signal processed by FFT and Envelope Analysis.

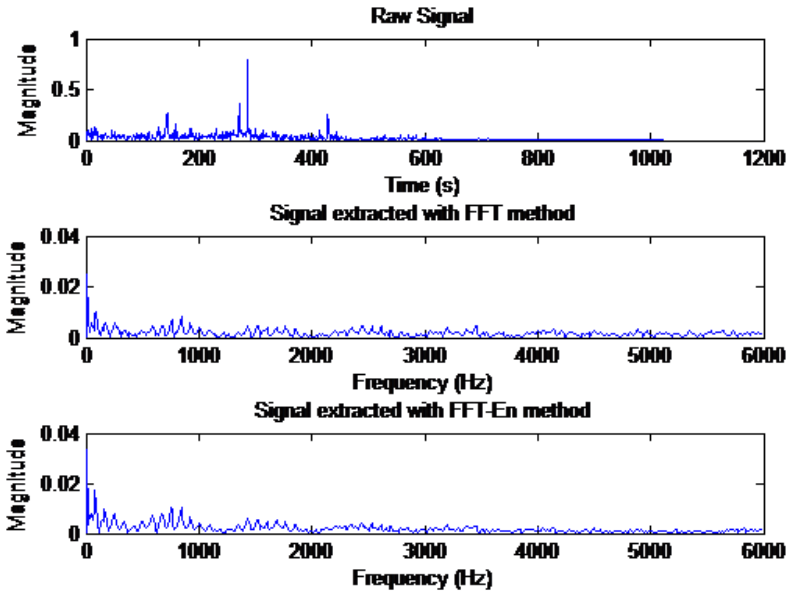

Fig. 3.3.3-b) FFT-En plot of a damaged SKF bearing

From these two figures, it can be observed that the signatures from healthy or faulty bearings collected from the same motor have different features. Therefore, the status of motor can be diagnosed by these features as shown in Chapter 4.

CHAPTER 4

INDEPENDENT COMPONENT ANALYSIS

4.1 Introduction

Feature extraction techniques select the relevant and useful information from a high dimensional space. Generally, feature extraction techniques are based on linear methods, for example, Linear Discriminant Analysis (LDA), Principal Component Analysis (PCA), and Independent Component Analysis (ICA).

Independent Component Analysis (ICA) belongs to a blind source separation algorithm, which transforms the high dimensional features into underlying components with rich information contents. ICA is commonly applied to biomedical signal processing [12], financial [13], medical area [14], and image processing [15]. However, ICA is relatively less known in the field of induction motor fault detection and diagnosis.

The aim of this thesis is to classify the type of motor faults by identifying the dominating feature. This Chapter will focus on the implementation of ICA.

Independent Component Analysis (ICA) is a technique that separates a class of blind multivariate source data into underlying informational components, which are mutually independent. The basic condition of ICA is that these components are independent in complete statistical sense and have non-Gaussian distributions.

ICA is an extension of Principal Component Analysis (PCA) that is also a multivariate technique. PCA is a statistical technique that linearly transforms an original set of

variables into a substantially smaller set of uncorrelated variables that represents most of the information in the original set of variables [16]. The main difference between ICA and PCA is that PCA focuses on uncorrelated and Gaussian components, and that is a weaker condition than statistically independent.

If covariance of two random variables (y_1 and y_2) is zero, they are said to be uncorrelated:

$$E\{y_1 y_2\} - E\{y_1\}E\{y_2\} = 0 \tag{4.1}$$

Being uncorrelated does not imply that the random variables are independent. On the contrary, if the variables are independent, they must be uncorrelated. Therefore, ICA is a more powerful tool than PCA.

ICA is capable of finding the underlying factors where classic methods fail completely. However, independent components in ICA must be non-Gaussian, because Gaussian variables do not contain any information, which will imply the directions of the full-rank or mixing matrix.

PCA is a transformation method based on correlation (second-order statistics) and orthogonal transformation. In contrast, not merely does ICA decorrelate the second-order statistics signals, it also reduces their dependencies in higher-order statistically. Therefore, ICA is a transformation technique of a linear non-orthogonal co-ordinate system in any random multivariate data, and the second and higher order statistics of the source data determines the directions of this co-ordinate system. The objective of ICA is to transform the variables of original data into a statistically independent set from each other.

ICA is proper to blind source separation or classification, and was designed to deal with the separation of a mixed signal problem. Recently, ICA is generally used in the signal processing field, such as fault diagnosis and feature extraction. In this thesis, ICA is applied as blind fault feature extraction method on different data sets collected as in Chapter 3.

4.1.1 Independence in ICA

A necessary step of ICA is to estimate the independent component matrix. In this thesis, independence of two scalar-valued random variables y_1 and y_2 is considered to be information of variable y_1 does not have any same information of variable y_2, and vice versa.

Mathematically, independence can be measured by probability densities. Equation (4.1.1.1) shows the joint probability density function of y_1 and y_2. If and only if this function is factorizable, random variables y_1 and y_2 can be said to be independent. This definition also can be extended for any number n-variables of random variables. In this case, the joint density must be number n terms product.

$$P(y_1, y_1) = P(y_1)P(y_2) \qquad (4.1.1.1)$$

If two random variables have zero-covariance, they are known to be uncorrelated. That implies a weaker condition of independence between these two variables as mentioned in Section 4.1. On the contrary, if these variables are uncorrelated, they are independent. Therefore, most ICA includes the estimation procedure. This procedure always gives independent components uncorrelated estimation. The advantage of the estimation

procedure in ICA is that it can reduce the number of free parameters and make the problem simply.

ICA finds the independent components by maximizing or minimizing the statistical independence of the estimated data. Cardoso [17] gives a review to provide the solutions for ICA problem of theoretic criteria of various measures, such as negentropy, mutual information, and maximum entropy.

In this thesis, mutual information method is used to measure the independence of random variables. Minimizing mutual information approximately is roughly equivalent to finding directions where the negentropy is maximized. That is to say, calculating mutual information method aims to find a one-dimensional subspace, in which the projection of mutual information has the maximum value of negentropy.

Projection pursuit is a technique used in statistics, to obtain "interesting" projections of multidimensional data. Mutual information connects the relationship between projection pursuit and ICA transformation. Projection of mutual information can be applied for optimal visualization of density estimation and regression of data. In one-dimensional subspace of projection pursuit, ICA attempts to find directions, in which projections of the data have interesting distributions. Projection pursuit helps ICA find the non-Gaussian direction for the estimation the independent components of data. Therefore, when all the non-Gaussian directions have been found by projection pursuit, all the independent components of the data will be estimated.

ICA estimation is performed by minimizing mutual information, which equals to maximize the sum of non-Gaussianities of the uncorrelated estimates. In this thesis an

effective method is used for finding the minimization of non-Gaussian directions to obtain ICA transform.

4.1.2 Data Preprocessing for ICA

To provide better results, ICA commonly use normalizing, centering, and whitening to preprocess the data initially. These preprocessing will now be described briefly below.

Normalizing:

Normalizing is a process that changes the amplitude range of raw signals values. This process normalizes the signals to have a common maximum amplitude, but does not change the relative magnitudes (or signatures) of these features. Therefore, this algorithm first finds out the maximum amplitude (recorded as λ) of each signal. Then the algorithm divides each signal by its maximum amplitude λ to get the normalizing results of signatures.

Centering:

Centering is a useful preprocessing strategy for ICA for transforming the input signatures to a zero-mean variable, so that all independent components will have zero-mean as such. The implementation of this algorithm is that it subtracts the mean ($E\{x\}$) from the observed variable x.

Whitening:

Whitening is another preprocessing algorithm in ICA to de-noise the measured data vector **x** by a linear transformation, to transform this vector into a new vector $\hat{\mathbf{x}}$, where its

components are mutually uncorrelated and all have equal unity variance. The purpose of whitening is to simplify the procedure of ICA by reducing the dimension of parameters, which will be estimated after whitening. Furthermore, this preprocessing not only reduces the complexity of ICA, but also avoids over-learning in ICA.

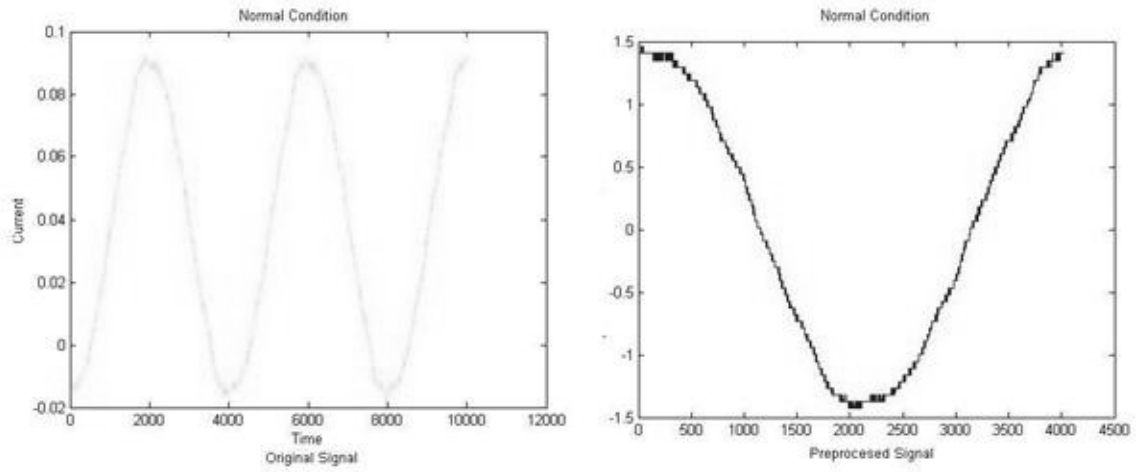

Fig. 4.1.2-a) The signal with normal condition before and after preprocessing

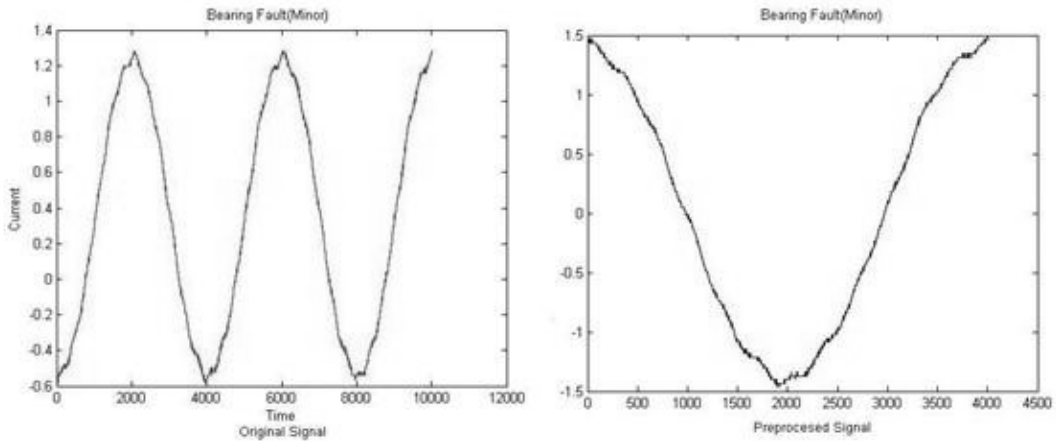

Fig. 4.1.2-b) The signal with bearing-fault before and after preprocessing

The above figures present two comparison groups. Fig. 4.1.2-a) [7] shows original and preprocessed signal with normal condition and Fig. 4.1.2-b) [7] provides bearing-fault signal and their preprocessing signal. These signals are just for demonstrating the necessity of preprocessing in ICA, and not belong to any data sets of this thesis.

From these figures, it can be seen that the range of the left-side graphs (the original signal) is from 0 to 10000, but the range of the right-side graphs (signal after preprocessing) is only 0-4000. That is to say, only processing one cycle of original signal is enough to extract ICA features. Therefore, preprocessing effectively removes the repeating part of original signature and simplifies the problem of ICA.

4.1.3 Fast-ICA

As mentioned before, ICA can be formulated as:

$$\boldsymbol{Y} = \boldsymbol{W}\boldsymbol{X}. \tag{4.1.3.1}$$

where $\boldsymbol{X}$ is n-dimensions measured signal vectors, $\boldsymbol{Y}$ is a set of statistically independent components, which are extracted from $\boldsymbol{X}$, and $\boldsymbol{W}$ is the transformation matrix. The independent components $\boldsymbol{Y}$ are developed by maximizing the independency with respect to $\boldsymbol{W}$.

FastICA is an efficient and robust method for independent component analysis. The algorithm is based on a fixed-point and iteratively maximizes non-Gaussianity to measure the statistical independence. For example, there is a unit vector $\boldsymbol{W}$, and the projection $\boldsymbol{W}^{\boldsymbol{T}}\boldsymbol{X}$ maximizes non-Gaussianity. This algorithm, also can be called as “approximated negentropy”, is a quantitative measure of non-Gaussianity.

Negentropy is defined as:

$$J(y) \approx [E\{G(y)\} - E\{G(v)\}]^2 \quad (4.1.3.2)$$

Here G is any non-quadratic function, and v is Gaussian variable, which is zero mean and unit variance.

Negentropy is obtained by differential entropy, and it is zero for a gaussian variable and always non-negative. In FastICA, the approximated negentropy is iteratively maximized on a fixed-point for finding the independent components with respect to W.

FastICA improves ICA for faster processing speed and reliability. FastICA uses the natural gradient rather than the gradient-descent algorithms. The natural gradient multiplies the gradient of the feed forward weight matrix $\boldsymbol{W}$ by a positive definite matrix $\boldsymbol{W^T W}$. Then it eliminates the matrix inversion to accelerate the convergence speed. Since the time complexity of convergence is at least $\Theta(n^3)$, the natural gradient is clearly much faster than the gradient-descent algorithms for obtaining the convergence when the environment does not very change fast. Moreover, FastICA is easy to use, because this algorithm does not need any learning rate or other adjustable parameters.

4.1.4 Formulation of the FastICA

The MATLAB code of data preprocessing and FastICA can be found in Appendix 2.4 and 2.5, respectively. FastICA can be simply presented as:

$$\boldsymbol{Y = W \cdot X} \quad (4.1.4.7)$$

$$\boldsymbol{X = A \cdot Y} \quad (4.1.4.8)$$

$\boldsymbol{W} \cdot \boldsymbol{A} = \boldsymbol{I}$ ($\boldsymbol{I}$ represents Identity Matrix) (4.1.4.9)

where $\boldsymbol{X}$ is signal vectors as algorithm input, $\boldsymbol{Y}$ is independent component matrix as algorithm output, and $\boldsymbol{W}$ and $\boldsymbol{A}$ are separating and mixing matrix respectively. The purpose of ICA is finding the separating matrix $\boldsymbol{W}$, and then performs linear transformation of vectors $\boldsymbol{X}$ and gets the output matrix $\boldsymbol{Y}$.

In Chapter 3, the vibration signature of induction motor has been processed by FFT-En , and the result ($\boldsymbol{F_{signals}}$) will be the input of FastICA.

$$\boldsymbol{F_{signals}} = \boldsymbol{A} \cdot \boldsymbol{ICs} \quad (4.1.4.1)$$

Here $\boldsymbol{ICs}$ is assumed as a set of mutually independent vectors, and $\boldsymbol{A}$ is a constant mixing matrix, which will be estimated.

By rearranging (4.1.4.1), the independent components $\boldsymbol{ICs}$ can be presented as:

$$\boldsymbol{ICs} = \boldsymbol{W} \cdot \boldsymbol{F_{signals}} \quad (4.1.4.2)$$

where $\boldsymbol{W}$ is the transformation matrix, which is the inverse matrix of $\boldsymbol{A}$

Therefore, the extracted statistically independent components $\boldsymbol{ICs}$ also can be expressed as following:

$$\boldsymbol{ICs} = \begin{bmatrix} IC1 \\ IC2 \\ IC3 \end{bmatrix} = \begin{bmatrix} ic11 & ic12 & \dots & ic1N \\ ic21 & ic22 & \dots & ic2N \\ ic31 & ic32 & \dots & ic3N \end{bmatrix} \quad (4.1.4.3)$$

Each ***ICi*** (i=1,2,3) of (4.1.4.3) has the same length as each of $F_{signals}$ in (4.1.4.2). The ***ICs*** reflect the characteristic of signatures $F_{signals}$. Therefore, ICs and signatures $F_{signals}$ are used to calculate features of induction motor signature:

$$F_{Features} = F_{signals} \cdot IC^T \quad (4.1.4.4)$$

Here $F_{Features}$ are the features of signatures $F_{signals}$ after FFT-En and FastICA.

All the magnitude information of induction motors affects the results of the FFT-ICA features - $F_{Features}$.

For instance, F_{signal_m} is the m^{th} signal of $F_{signals}$ in frequency domain:

$$F_{signal_m} = (a_m(\omega 1)\ a_m(\omega 2) \ldots\ a_m(\omega N)) \quad (4.1.4.5)$$

Here $a_m(\omega i)$ $(i = 1,2, \ldots, N)$ expresses the magnitude information of component ωi $(i = 1,2, \ldots, N)$.

F_{signal_m} is transformed to a *M*-D feature by multiplied independent components ICs in (4.1.4.3) and given in the form as below:

$$(F_{signal_{m1}}\ F_{signal_{m2}} \ldots\ F_{signal_{mM}}) = F_{signal_m} \times \begin{pmatrix} ic_{11} & ic_{12} & \ldots & ic_{1N} \\ ic_{21} & ic_{22} & \ldots & ic_{2N} \\ \ldots & \ldots & \ldots & \ldots \\ ic_{M1} & ic_{M1} & \ldots & ic_{MN} \end{pmatrix}^T \quad (4.1.4.6)$$

where $F_{signal_{mj}}(j = 1,2,\dots,M)$ are respectively the FastICA feature from 1 to M of the m^{th} signal F_{signal_m}. Therefore, F_{signal_m} contains the magnitude information of each component in selected frequency domain.

Since $\ll N$, a high dimension signature of vibration signature F_{signal_m} in frequency-domain is mapped into a lower dimension feature $F_{signal_{mj}}(j = 1,2,\dots,M)$. In this thesis, two independent components are enough to diagnosis the status of induction motors.

4.2 Feature Extraction and ICA Plot

As mentioned in Chapter 2, vibration signals of induction machines are collected from the three sources: CWRU, Vestas and SKF Company. In this thesis, the features of these signatures are extracted by FastICA. The following Sections 4.2.1-4.2.3 will present a holistic view of the health and faulty signature database by feature extraction information.

This Chapter just presents part of feature extraction results. Chapter 6 will summarize and analyze the remaining results.

4.2.1 ICA Plot of CWRU Data sets [8]

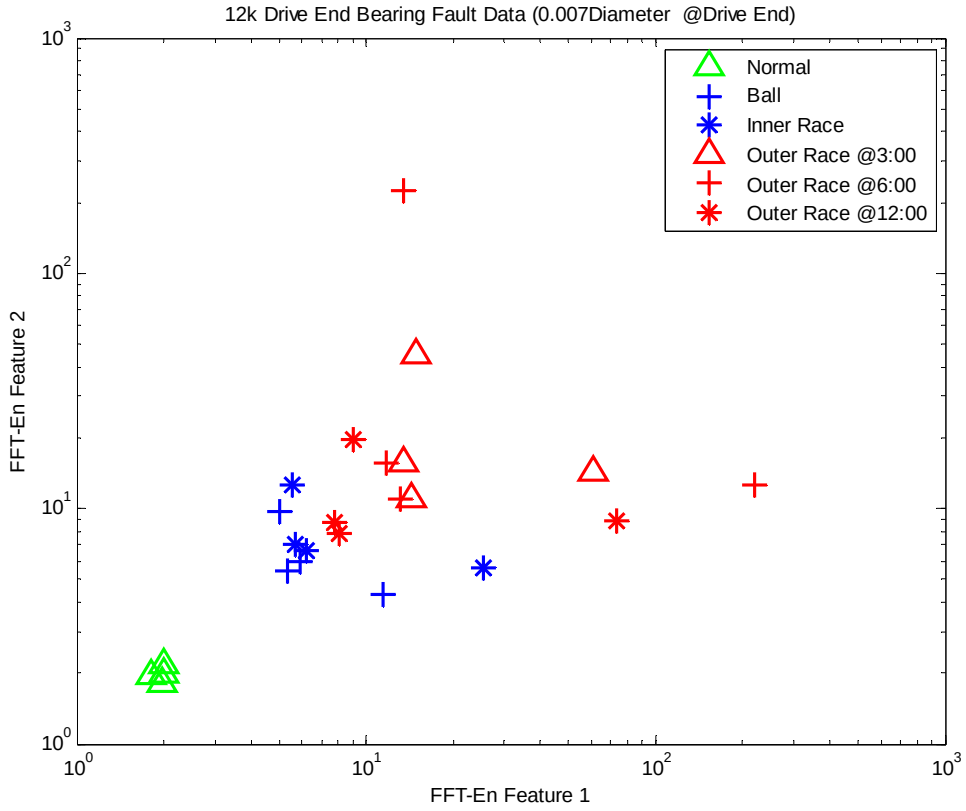

Fig. 4.2.1 ICA plot for CWRU data sets

In this figure, the normal signals shown as green triangle cluster at the bottom left-hand corner of the plot, the faulty signals are located at the opposite corner, and all the signals are situated around the 45 degree straight line. Therefore, the figure clearly classifies the status of induction motor (healthy or fault) by using two ICA features of signal.

4.2.2 ICA Plot of Vestas sets

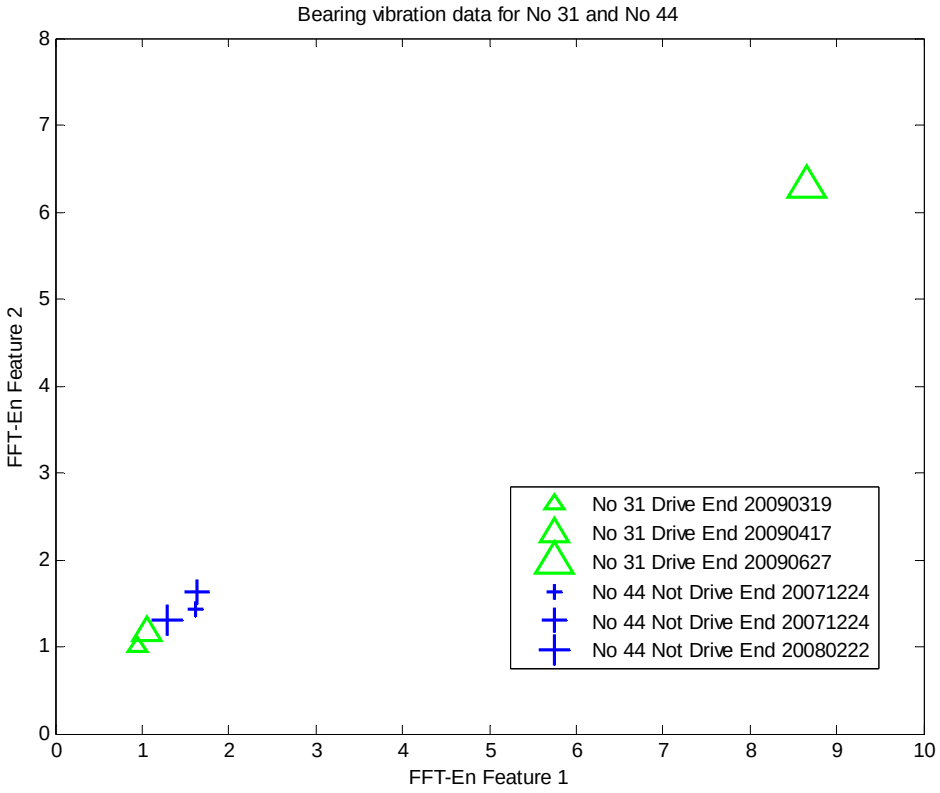

Fig. 4.2.2 ICA plot for Vestas data sets

In Fig. 4.2.2, two groups of ICA results are presented. The signatures shown as green triangles are collected from a faulty wind turbine No. 31, and others signatures illustrated as blue cross are collected from a health wind turbine No. 44.

Wind turbine No. 44 is healthy from start to finish, and Wind turbine No. 31 was damaged since the end of June 2009. In the figure, all the health signals cluster at the bottom left-hand corner, and the faulty one shown as the biggest green triangle is situated at the upper right-hand corner. Furthermore, all the signals are roughly located on the 45

degree straight line of this graph, which suggests the use of only one ICA feature for adequate fault classification.

4.2.3 ICA Plot of SKF Data sets

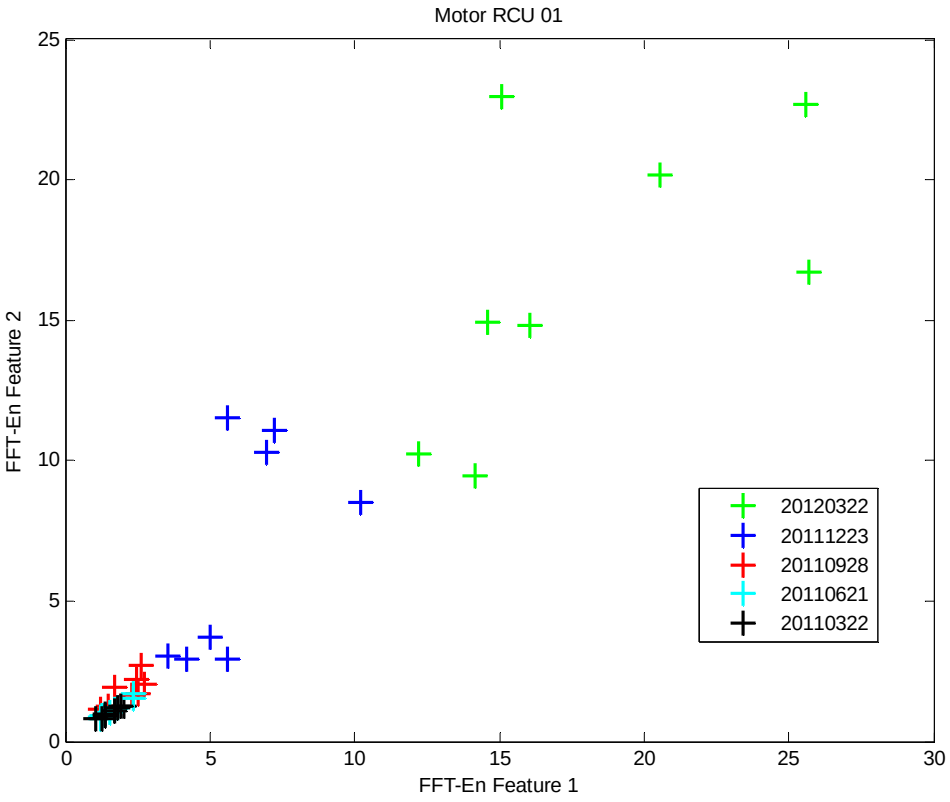

Fig. 4.2.3 ICA plot for SKF data sets

Fig. 4.2.3 demonstrates the ICA plot of on motor RCU01 provided by SKF. The signals are collected at 5 different times, and the motor is seen to have demonstrated worse performance with time since December 2011.

All the signals are situated round the 45 degree straight line of the plot. ICA clearly classifies between the healthy and fault signatures. Normal signals cluster at the bottom

left-hand corner of plot on a 45-degree line, and the faults signals migrate with time towards the other top right-hand corner of the plot.

CHAPTER 5

SUPPORT VECTOR MACHINE

5.1 Introduction

Support Vector Machine (SVM) is a relatively new machine-learning method, which is based on the statistical learning theory invented by Vladimir Vapnik and co-workers at AT&T Bell Labs in 1999 [18].

SVM is widely used in classification problem of varieties of disciplines as neural networks technique, such as biomedical [19], chemical process [20], financial analysis [21], image processing and face recognition [22], etc. The application SVM as well as intelligent system is reported in condition monitoring and fault detection of induction motor for faults classification. For instance, gear faults detection [23], bearing's ball-faults detection [24], cavitation detection of butterfly valve [25], condition classification of small reciprocating compressor [26], and so on.

5.1.1 Data Preparation for SVM

Before doing SVM, inputs data need special transformation for guaranteeing the good performance of classification. The feature extraction or feature selection is generally used for preparation of data inputs, which will be inputted into the SVM classifier.

The key reason of preparation data instead of directly inputting them into classifier is that large vibration data collected from induction motor have too many features. Most of

these features are usually irrelevant and redundant that will degrade the performance of classifier and cause problem of dimensionality phenomenon. Therefore, feature extraction or feature selection method is necessary to avoid the redundancy. As discussed in last Chapter, ICA, one of feature extraction methods, is selected to extract the useful features from vibration signals of frequency-domain.

5.1.2 Classification of SVM

In neural networks, SVM supervised learning model constructs a hyperplane / a set of hyperplanes in a high dimensional space for classification or regression analysis.

Given data set Σ containing ($N + \bar{N}$) samples is partitioned into two sets:

A training set: $S = \{(x_1, d_1), \ldots, (x_N, d_N)\}$ (5.1.2.1)

A test set: $\bar{S} = \{(\bar{x}_1, \bar{d}_1), \ldots, (\bar{x}_{\bar{N}}, \bar{d}_{\bar{N}})\}$ (5.1.2.2)

where $\Sigma = S \cup \bar{S}$, with $S \cap \bar{S} = \emptyset$. d_i ($i = 1,2, \ldots, N \text{ or } \bar{N}$) is the label of each sample, which be $d_i = -1$ for healthy class and $d_i = 1$ for fault class, respectively. Training data set S is for constructing SVM, and test data set $\bar{S}$ is for evaluating performance of SVM.

In the case of linearly data, a hyperplane, which can separate the given data, denoted by *(**w**, b)*, can be expressed as:

Discriminant function: $g(\boldsymbol{x}) = \boldsymbol{w}^T \boldsymbol{x} + b = 0$ (5.1.2.3)

This is the decision function here w is N-dimensional vector and b is a scalar, and they are used to define the position of hyperplane. One side of hyperplane belongs to healthy class and the other side is fault class.

Separating hyperplane classifies a given xi with

$$sgn\,[g(x_i)] = \begin{cases} +1 & if \;\; g(x_i) > 0 \\ -1 & if \;\; g(x_i) < 0 \end{cases} \qquad (5.1.2.4)$$

Hyperplane classifies an example (x_i, d_i) correctly if $sgn\,[g(x_i)] = d_i$, the processing is shown as Fig. 5.1.2-a).

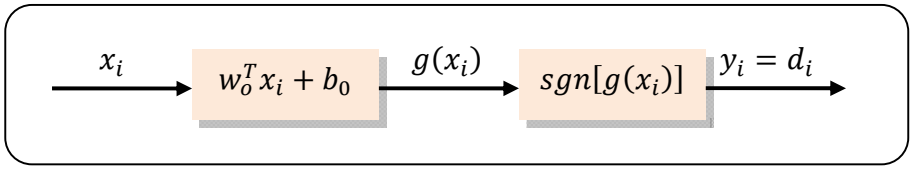

Fig. 5.1.2-a) Steps of classification of SVM

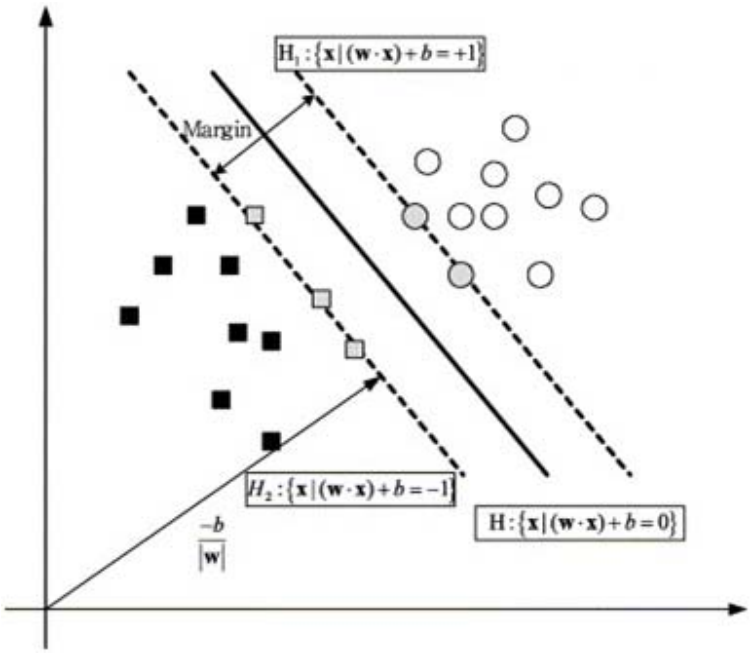

Fig. 5.1.2-b) Classification using SVM

There are many possible separating hyperplanes for classification, but there is only one optimal hyperplane, which produces the maximum margin between the plane and the nearest data. Fig. 5.1.2-b) [27] illustrates an optimal separating hyperplane for linear classification between two classes. Therefore, finding the maximum margin between the two different classes is the key to find optimal hyperplane.

The function margin of an example (x_i, d_i) with respect to a hyperplane $(\boldsymbol{w}, b)$ is defined as:

$$\gamma_i^f = d_i(\boldsymbol{w}^T x_i + b) \tag{5.1.2.5}$$

The geometric margin of an example (x_i, d_i) with respect to a hyperplane $(\boldsymbol{w}, b)$ is defined as:

$$\gamma_i^g = d_i(\frac{1}{\|\boldsymbol{w}\|}\boldsymbol{w}^T x_i + \frac{1}{\|\boldsymbol{w}\|} b) \tag{5.1.2.6}$$

The functional margin of a training set $\boldsymbol{S}$, with respect to a hyperplane $(\boldsymbol{w}, b)$ is the minimum of all the function margin of the individual examples in $\boldsymbol{S}$, i.e.,

$$\gamma^f = min_{1\le i\le N}\{\gamma_i^f\} \tag{5.1.2.7}$$

The geometric margin of a training set $\boldsymbol{S}$, with respect to a hyperplane $(\boldsymbol{w}, b)$ is the minimum of all the geometric margin of the individual examples in $\boldsymbol{S}$, i.e.,

$$\gamma^g = min_{1\le i\le N}\{\gamma_i^g\} \tag{5.1.2.8}$$

Therefore, the relationship between the functional margin and the geometric margin of a training set $\boldsymbol{S}$ is:

$$\gamma^g = \frac{\gamma^f}{\|\boldsymbol{w}\|} \quad (5.1.2.9)$$

To find the optimal hyperplane with the maximum margin, γ^g is maximized by fixing γ^f then minimizing $\|\boldsymbol{w}\|$.

Therefore, the optimal separating hyperplane can be found as following constrained optimization problem [27]:

Minimizing: $f(\boldsymbol{w}) = \frac{1}{2}||\boldsymbol{w}||^2 = \frac{1}{2}\boldsymbol{w}^T\boldsymbol{w}$ (5.1.2.10)

Subject to: $d_i(\boldsymbol{w}^T\boldsymbol{x}_i + b) \geq 1\,, \quad for\ i = 1,2,\dots,N$ (5.1.2.11)

Equation (5.1.2.10) and (5.1.2.11) can be alternated with Karush-Kuhn-Tucker (KKT) condition [28] by using method of Lagrange multipliers [29] [30]:

Minimizing: $L(\boldsymbol{w}, \boldsymbol{\alpha}, \boldsymbol{\beta}) = f(\boldsymbol{w}) + \sum_{i=1}^{k} \alpha_i q_i\,(\boldsymbol{w}) + \sum_{i=1}^{m} \beta_i h_i(\boldsymbol{w})$ (5.1.2.12)

Subject to: $\frac{\partial L(\boldsymbol{w}_o, \boldsymbol{\alpha}_o, \boldsymbol{\beta}_o)}{\partial \boldsymbol{w}} = 0, \quad \alpha \geq 0$

Here α_i and β_i are the Lagrange multipliers. The problem is minimizing (5.1.2.12) with respect to **w** and *b*

Consider the KKT condition:

$$\frac{\partial L(\boldsymbol{w}, \boldsymbol{\alpha}, \boldsymbol{\beta})}{\partial \boldsymbol{w}} = 0 \quad (5.1.2.13)$$

$$\frac{\partial L(\boldsymbol{w}, \boldsymbol{\alpha}, \boldsymbol{\beta})}{\partial b} = 0 \quad (5.1.2.14)$$

Therefore:

$$\boldsymbol{w} = \sum_{i=1}^{N} \alpha_i d_i \boldsymbol{x}_i \quad (5.1.2.15)$$

$$\sum_{i=1}^{N} \alpha_i d_i = 0 \quad (5.1.2.16)$$

where $\boldsymbol{w}$ is contained by $\boldsymbol{x_i}$ in the subspace spanned. Then by replacing (5.1.2.15) and (5.1.2.16) into (5.1.2.12), the dual quadratic optimization hyperplane can be expressed as following:

Maximizing: $L(\alpha) = \sum_{i=1}^{N} \alpha_i - \frac{1}{2}\sum_{i=1}^{N}\sum_{j=1}^{N} \alpha_i \alpha_j d_i d_j \boldsymbol{x}_i{}^T \boldsymbol{x}_j$ (5.1.2.17)

Subject to: (1) $\sum_{i=1}^{N} \alpha_i d_i = 0$

(2) $\alpha_i \geq 0, \quad (i = 1, 2, \ldots, N)$ (5.1.2.18)

Thus, finding Lagrange multipliers $\{\alpha_i\}$, expressed the $\boldsymbol{w}$ to solve (5.1.2.10), is the key to solve the dual optimization problem.

5.2 Training and Classification

Since SVM needs abundant training data for constructing SVM, data sets from Vestas and SKF Company are not large enough to train SVM, this thesis will only process CWRU data sets by SVM.

Two groups of samples have been selected from the CWRU data set to form a training set (with 37 samples). Another group of 37 samples are then selected from the remaining samples in the CWRU data set to form a test set. Each sample has 2 features that have been computed by ICA feature extraction.

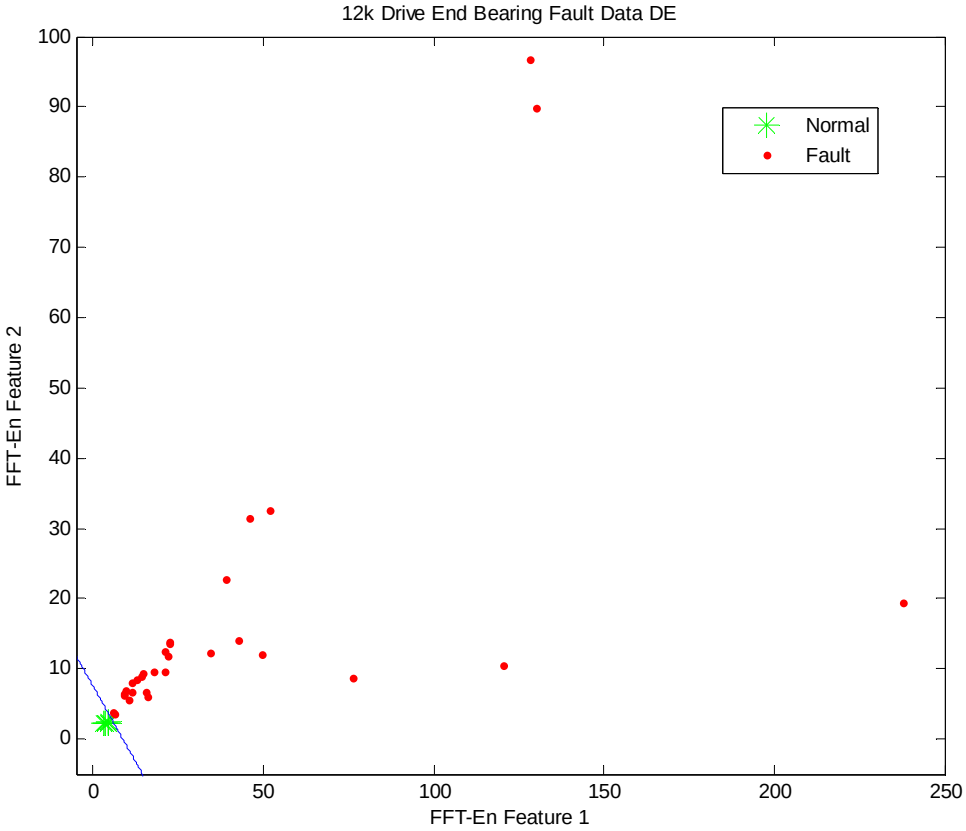

Fig. 5.2-a) SVM plot of training set

Fig. 5.2-a) presents the SVM training results. The green stars are normal signals, and the red points represent all bearing faulty signals including ball-fault, inner race fault and outer race fault. The blue straight line is placed as a linear boundary between the two different groups.

To show the classification more clearly, Fig. 5.2-b) zooms the boundary part of Fig. 5.2-a). From this figure, it can be seen that health signatures and faulty signatures are completely separated by the SVM in the linear classification.

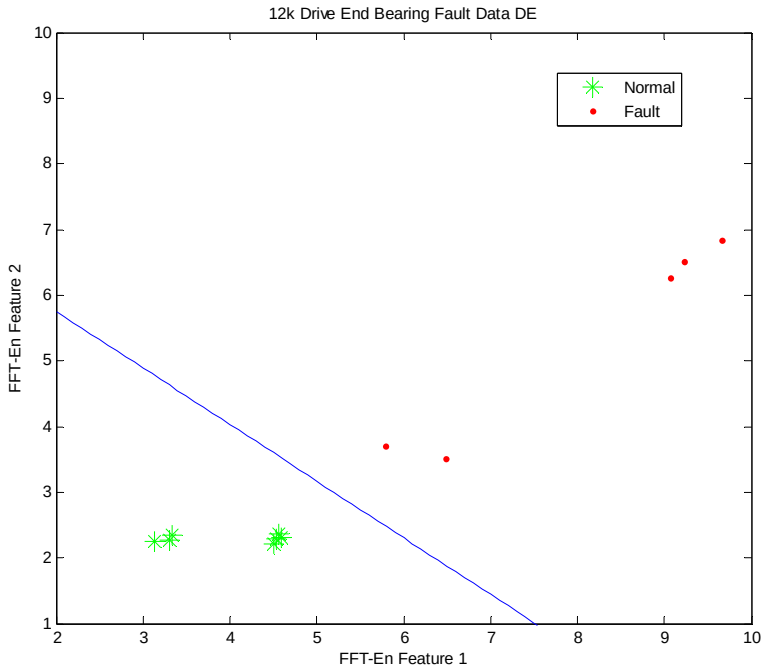

Fig. 5.2-b) Zoom plot of training set SVM result

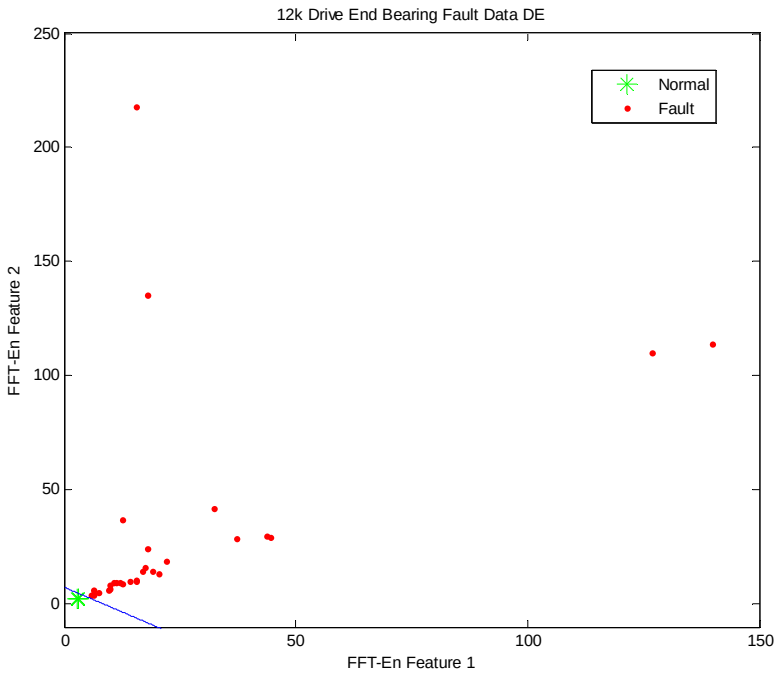

Fig. 5.2-c) SVM plot of test set

Fig. 5.2-c) is a plot of the SVM test results. The blue straight line, which is the same as the line in Fig. 5.2-a), is calculated by the processing of SVM training. It successfully classifies the normal signals (green stars) and the bearing faulty signals (red points).

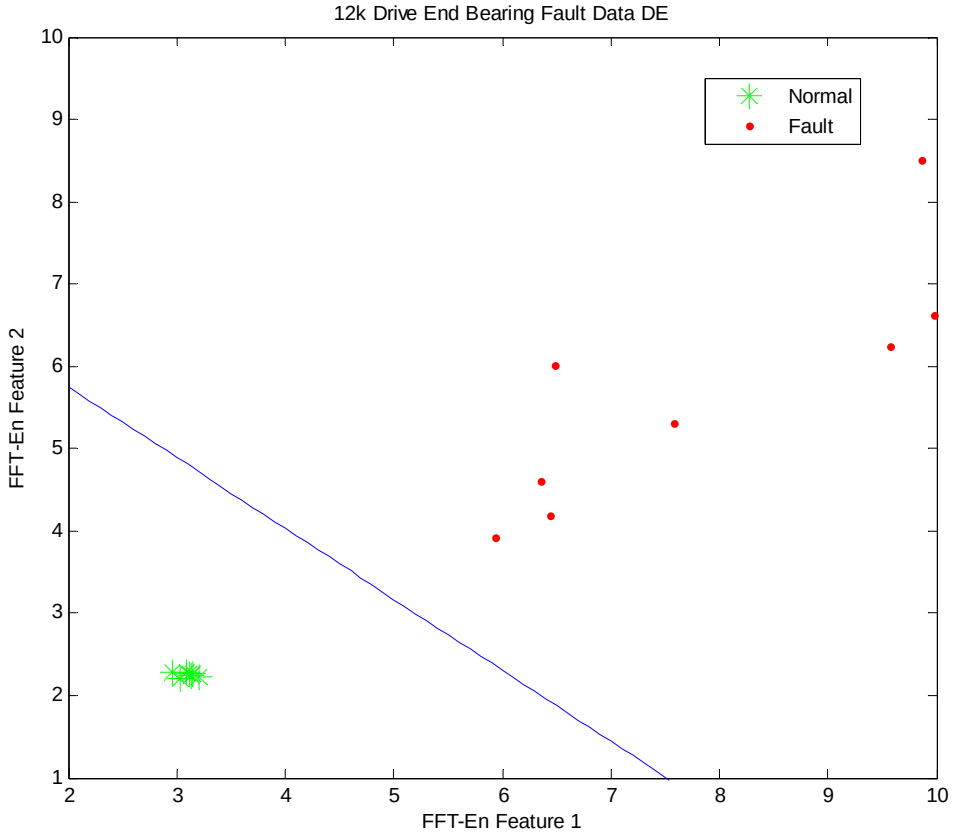

Fig. 5.2-d) Zoom plot of test set SVM result

Fig. 5.2-d), zoom graph of Fig. 5.2-c), indicates that SVM can automatically diagnose the status of induction motor bearing by separating signatures into two classes according to their features.

CHAPTER 6

PROPOSED FAULT CLASSIFICATION PLATFORM AND RESULTS

6.1 System Scheme

Fig. 1.3 shows linkages in the proposed platform between various the algorithms, which have been described in previous Chapters of this thesis. The platform has four functional steps, which are described as follows:

Firstly, the raw vibration signal in MATLAB data format (*.m) is inputted into the training system. Signals are in time-domain and include all types of bearing faults, for example, ball-fault, inner race fault and outer race fault.

Secondly, the raw vibration signals are transformed from the time-domain to frequency-domain by FFT using the magnitudes of the selected frequency components.

Thirdly, signatures in frequency-domain are processed by Envelope Analysis for extracting the related characteristics of signals from high frequency modulation signatures and reducing the noise influence. The function of Envelope Analysis is to find fault signal band and envelope spectrum analysis in the signal band.

Fourthly, the extracted signatures are inputted into ICA to select the signatures from high dimensional space into underlying informational components. According to the

dominating feature of signatures, ICA separates them into two groups with one being normal signatures and the other one being faulty.

Using the above data group as the training data sets, test signatures are entered into the system and processed as training signatures (from steps 1^{st} to 4^{th}).

Given the test set after further data collection, both ICA features of the training set and ICA features of the test set are directly loaded into SVM. Each of these two data sets contains two variables: the matrix variable data, in which each column represents one sample signal, and the variable label, which contains the class label (i.e., −1 for Healthy Signal and+1 for Fault Signal) of the samples. SVM classifies the given training set and test set, plots classification results of these two data sets, and calculates the classification rates with ICA feature extraction. Furthermore, the procedure of test data classification is automatic processing of detection and diagnosis of induction motor condition.

6.2 Project Results and Discussion

6.2.1 Summary of Results for CWRU [8]

Results of CWRU data sets are seen in Table 6.2.1, which lists the classification rates for training and testing of the 6 experimental data sets.

Table 6.2.1 Accuracy of fault classification using SVM (%)

	Drive-end (fs:12k, DE)	Drive-end (fs:12k,FE)	Drive-end (fs:48k,DE)	Drive-end (fs:48k,FE)	Fan-end (fs:12k,DE)	Fan-end (fs:12k,FE)
Training	100	100	100	100	100	100

Testing	100	87.88	100	100	100	100

The accuracy of classification is defined as following:

Classification rate = the number of correct classification/ the whole sample size of training or test set

The classification rate of this process as shown in this table is nearly 100%.

Fig. 6.2.1-a)-c) show the classification results of drive-end motor bearing test. Experiments are processed using a 2 hp Reliance Electric motor, and acceleration data is collected at locations near to fan-end at 12,000 samples per second. The test set classification rate of this data set is 87.88%, and the sample size of the test set is 33. That is to say, the number of wrong classifications of the test set is four.

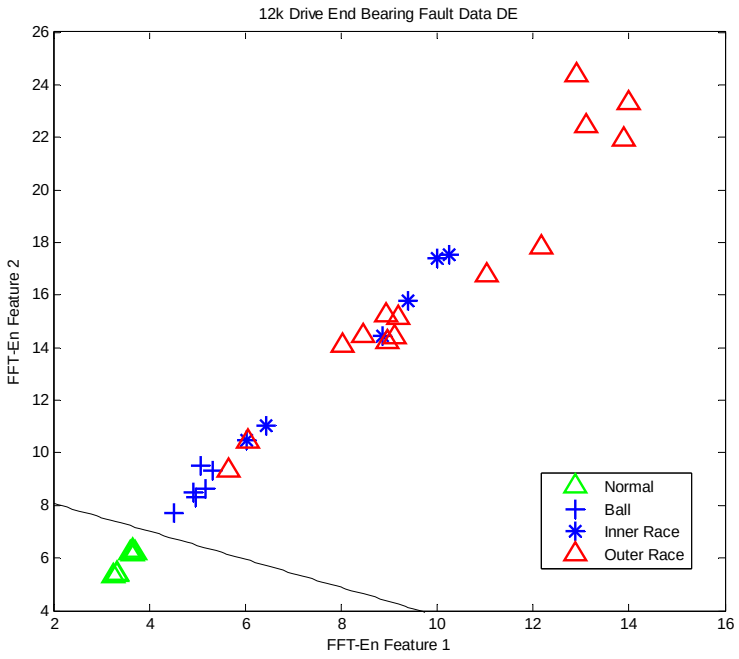

Fig. 6.2.1-a) SVM plot for training set

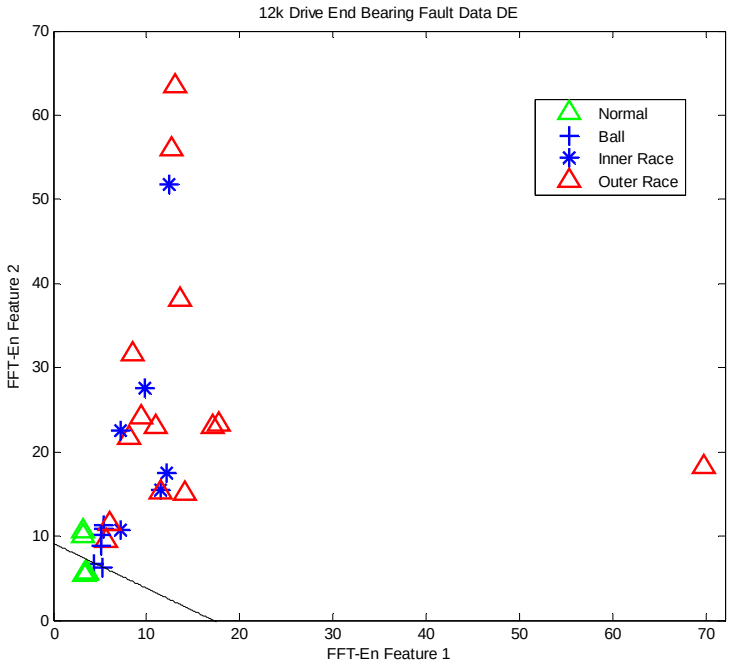

Fig. 6.2.1-b) SVM plot for test set

From Fig. 6.2.1-c), it can be seen that two healthy signatures as green triangle and two ball-fault signatures as blue cross are misclassified. One of the reasons for this result is that the sample size of training set is not big enough to train SVM well. Large data volumes for training are necessary for constructing SVM, so that the boundary between the health class and fault class will be clearer, and when new test data are loaded, their classification rate will be higher.

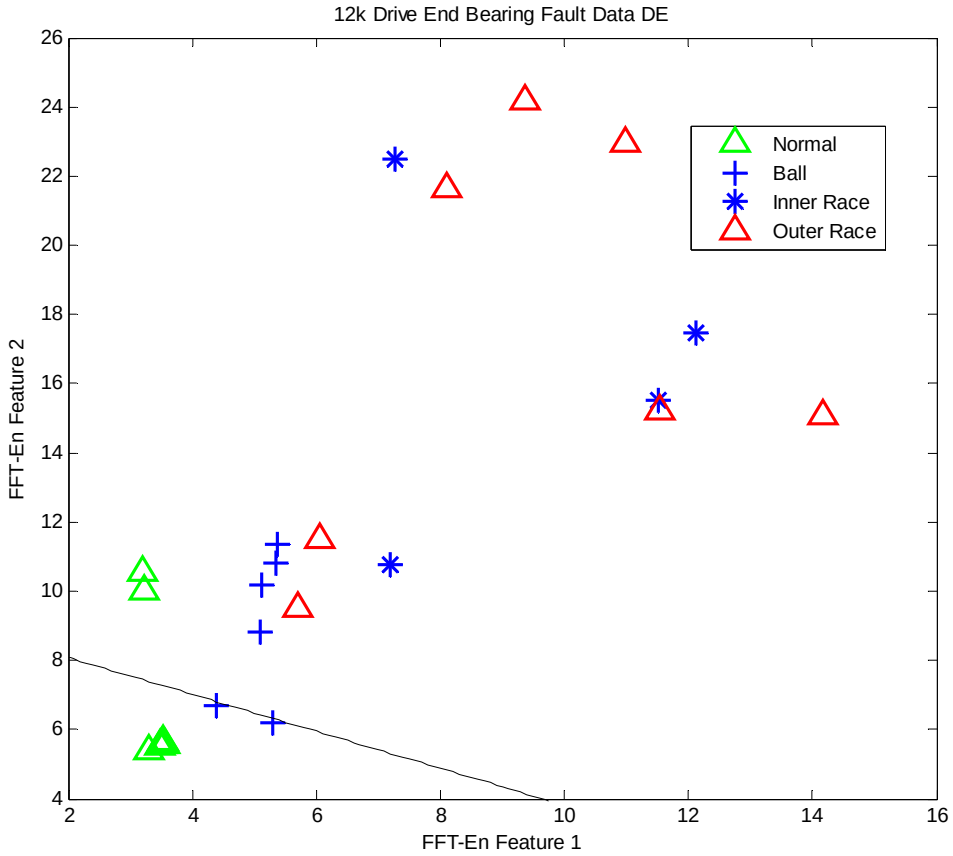

Fig. 6.2.1-c) Zoom of SVM plot for test set

The other reason is this thesis only uses 2 real-valued features of each signal in SVM. These features are extracted by ICA from induction motor vibration signatures. As shown in Section 4.2, two features of each signal are good enough to detect the condition of induction motor. However, some of the healthy data of the test data move away from the lower left-hand corner of the plot. In this case, more features should be used to recreate SVM.

However, the accuracies of this study for diagnosis of induction motor is sufficiently high, and using ICA as preprocessing algorithm of SVM is useful and efficient.

6.2.2 Results for Vestas

The number of data sets of Vestas Company is not large enough to construct SVM, but the results of ICA are extremely clear to diagnose the status of wind turbine.

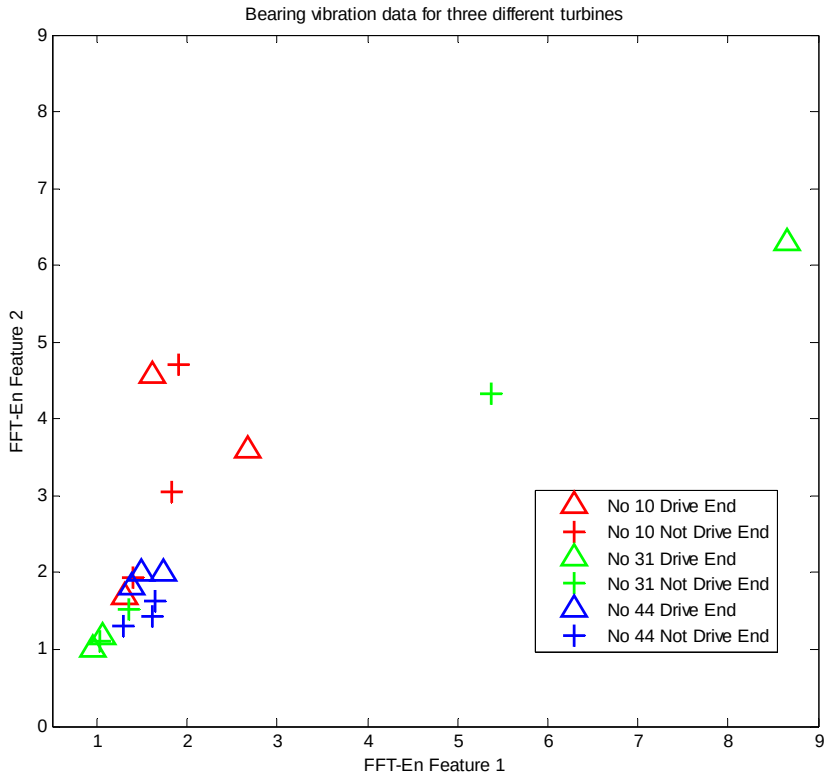

Fig. 6.2.2-a) Classification of Vestas data sets using ICA

Fig. 6.2.2-a) presents the features of signatures of three different wind turbine. To get better view, this figure is transform into 3D coordinate space shown as Fig. 6.2.2-b). From this Figure, the signatures of wind turbine No. 44 shown as blue are concentrated at the corner of the origin coordinates, part of the signatures of wind turbine No. 31 shown as green are concentrated at the bottom corner and two of them away from this corner,

and all of the signatures of wind turbine No. 10 shown as red are scattered at the opposite direction of the origin coordinates.

Therefore, this thesis succeeds with detection of the condition of wind turbine. Wind turbine No. 44 is healthy, Wind turbine No. 10 is broken, and Wind turbine No. 31 is broken during the measure period.

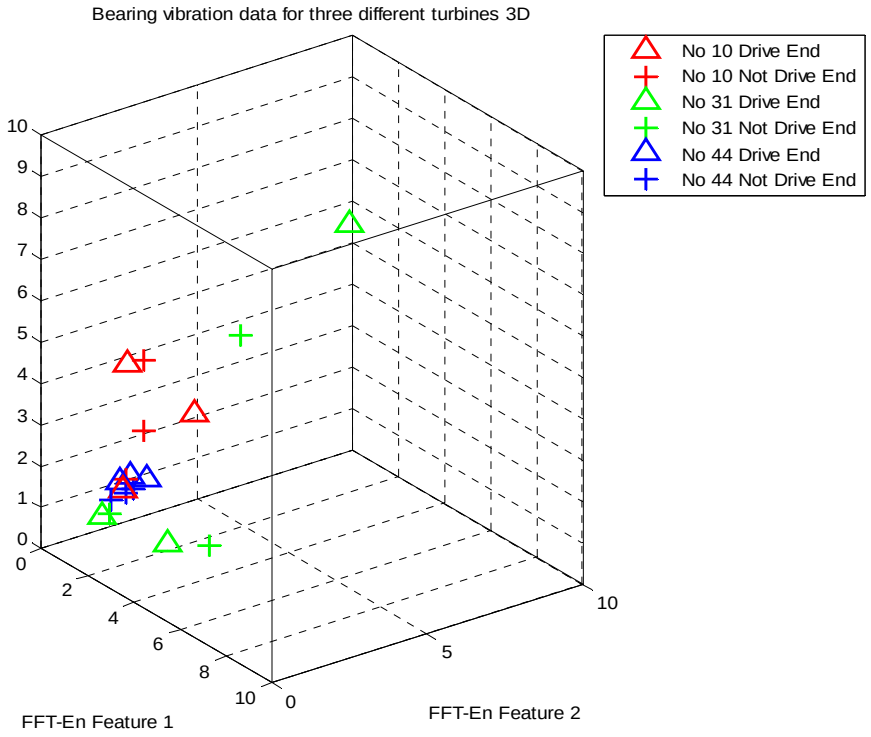

Fig. 6.2.2-b) Classification of Vestas data sets using ICA in 3dimension

6.2.3 Results for SKF data sets

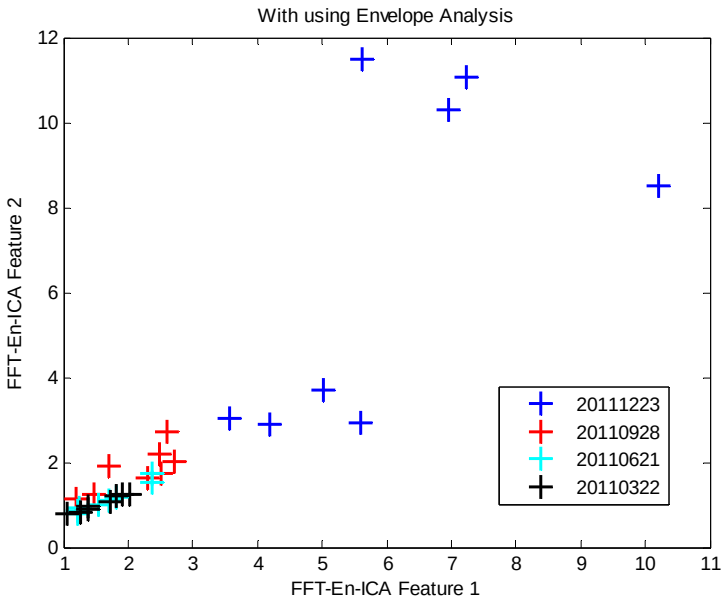

Fig. 6.2.3-a) Classification of SKF data sets using FFT-En-ICA

Fig. 6.2.3-a) presents the plot of ICA features, which have been extracted by FFT and Envelope Analysis. As mentioned in Section 4.2.3, this motor RCU01 was healthy until December 2011. In this figure, all the signals are situated round the 45 degree straight line of the plot, normal signals cluster is at the bottom left-hand corner of plot, and the faults signals cluster is towards the other top right-hand corner of the plot.

Fig. 6.2.3-b) demonstrates the plot of ICA features extracted from the same motor RCU01 as used in Fig. 6.2.3-a). However, the method of extraction is only using FFT. In this figure, normal signals are at the bottom of the plot, and the faults signals are at the top of the plot. The classification of this figure is not clear as Fig. 6.2.3-a). When the condition of the motor is unknown, it is difficult to make a correct diagnosis just according to FFT-ICA features. Due to Envelope Analysis can significantly reduce the

influence of signature noise, the hybrid method of FFT and Envelope analysis can more efficiently extract the fault features.

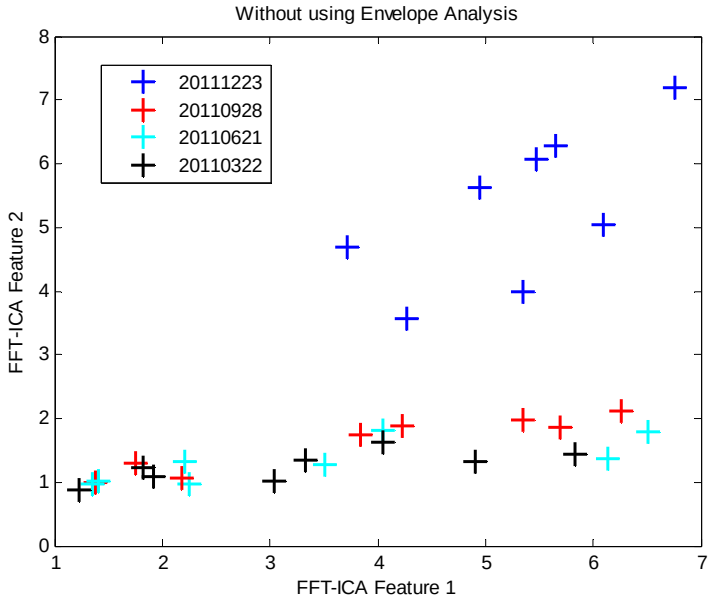

Fig. 6.2.3-b) Classification of SKF data sets only using FFT-ICA

CHAPTER 7

CONCLUSION

7.1 Outcomes

This thesis addresses application of computational intelligence for fault detection of induction machines and electromechanical systems. The method of fast Fourier transform and Envelope Analysis is applied to the vibration waveforms measured from a set of healthy and faulty induction motors for converting the time-domain signals into the frequency domain. Independent component analysis is then applied to the resulted frequency spectrums for extracting their dominant features from each healthy or faulty motor. The support vector machine is finally applied for classifying patterns obtained from these electric motors for detecting bearing problems from the faulty motors. Extensive studies have been conducted to evaluate the performance of fault detection and diagnosis of induction machines.

In this thesis, the integration of FFT and Envelope Analysis is proposed to the vibration signatures measured. Envelope Analysis based on Hilbert transformation not only extracts the useful signatures from the high frequency modulation signature, but also reduces the noise influence in signals. The hybrid method of FFT and Envelope Analysis has efficiently extracted the fault features.

Quantification feature extraction method can improve the reliability and performance of fault detection and diagnosis results. This thesis uses ICA as feature extraction method.

ICA is simple and reliable to extract the relative features from the signatures in frequency-domain, and does not require any prior knowledge of induction machine parameters for fault detection and diagnosis. That is to say, ICA can monitor the condition of induction machine just using a set of healthy and faulty signatures collected from this machine instead of using information of machine parameters.

This thesis is not only applicable to induction motor's condition monitoring and fault detection, and can also detect and diagnose the condition of electromechanical systems. As mentioned in Section 6.2.2, this thesis presents the successful detection results of three wind turbines of Vestas.

In conclusion, this thesis introduced a new fault detection and diagnosis of induction machines and electromechanical system based on fast Fourier transform, Envelope Analysis, independent component analysis and support vector machine of vibration signatures. The new system was tested with experimental data collected from sensor measuring the vibration from three groups: the Bearing Data Center of Case Western Reserve University, Vestas R&D Centre in Singapore and SKF. The system is a robust and effective for fault detection and diagnosis of induction machines and electromechanical systems.

7.2 Future Work

Most vibration data sets studied in this thesis were collected from bearings. However, there are still some other common faults in induction motors, such as rotor bar fault, gear faults, mechanical looseness, imbalance in motor load, and so on. In the future, these

types of induction motor faults should be established on laboratory motors, and be detected and diagnosed by FFT-En and ICA-SVM.

To classify more classes of motor faults, this system will improve SVM. Because there are only two types of motor status for detection in this thesis, which are linearly separable, this system uses linear and hard-margin SVM for classification. In future research, SVM with characteristics of non-linear, soft-margin, and multi-class classification should be developed. More powerful SVM classification will help the system to become a more functional motor fault technique, which should be used in other induction motor detection and diagnosis.

In addition, features of composite bearing faults (ball-fault, inner race fault, and outer race fault) can be mixed. To solve this problem, Zoom-FFT should be developed and integrated into this system. Spectra component of signatures, which can detect the condition of induction motor commonly lie in a certain frequency window. Zoom-FFT can find these windows and extract the features of signature better and faster. Therefore, Zoom-FFT should be built for more robust detection of induction motor faults in the future study.

APPENDICES

A.1 CWRU Vibration data Information [8]

Table A.1-a) 12k drive-end bearing-fault data

Fault Diameter (inches)	Motor Speed (rpm)	Inner Race	Ball	Outer Race Position Relative to Load Zone (Load Zone Centered at 6:00)		
				Centered @6:00	Orthogonal @3:00	Opposite @12:00
0.007"	1797	I07_0	B07_0	O07@6_0	O07@3_0	O07@12_0
	1772	I07_1	B07_1	O07@6_1	O07@3_1	O07@12_1
	1750	I07_2	B07_2	O07@6_2	O07@3_2	O07@12_2
	1730	I07_3	B07_3	O07@6_3	O07@3_3	O07@12_3
0.014"	1797	I14_0	B14_0	O14@6_0		
	1772	I14_1	B14_1	O14@6_1		
	1750	I14_2	B14_2	O14@6_2		
	1730	I14_3	B14_3	O14@6_3		
0.021"	1797	I21_0	B21_0	O21@6_0	O21@3_0	O21@12_0
	1772	I21_1	B21_1	O21@6_1	O21@3_1	O21@12_1
	1750	I21_2	B21_2	O21@6_2	O21@3_2	O21@12_2
	1730	I21_3	B21_3	O21@6_3	O21@3_3	O21@12_3
0.028"	1797	I28_0	B28_0			
	1772	I28_1	B28_1			

	1750	I28_2	B28_2			
	1730	I28_3	B28_3			

Table A.1-b) 48k drive-end bearing-fault data

Fault Diameter (inches)	Approx. Motor Speed (rpm)	Inner Race	Ball	Outer Race Position Relative to Load Zone (Load Zone Centered at 6:00)		
				Centered @6:00	Orthogonal @3:00	Opposite @12:00
0.007"	1797	I07_0	B07_0	O07@6_0	O07@3_0	O07@12_0
	1772	I07_1	B07_1	O07@6_1	O07@3_1	O07@12_1
	1750	I07_2	B07_2	O07@6_2	O07@3_2	O07@12_2
	1730	I07_3	B07_3	O07@6_3	O07@3_3	O07@12_3
0.014"	1797	I14_0	B14_0	O14@6_0		
	1772	I14_1	B14_1	O14@6_1		
	1750	I14_2	B14_2	O14@6_2		
	1730	I14_3	B14_3	O14@6_3		
0.021"	1797	I21_0	B21_0	O21@6_0	O21@3_0	O21@12_0
	1772	I21_1	B21_1	O21@6_1	O21@3_1	O21@12_1
	1750	I21_2	B21_2	O21@6_2	O21@3_2	O21@12_2
	1730	I21_3	B21_3	O21@6_3	O21@3_3	O21@12_3

Table A.1-c) 12k fan-end bearing-fault data

Fault Diameter (inches)	Approx. Motor	Inner Race	Ball	Outer Race Position Relative to Load Zone (Load Zone Centered at 6:00)

	Speed (rpm)			Centered @6:00	Orthogonal @3:00	Opposite @12:00
0.007"	1797	I07_0	B07_0	O07@6_0	O07@3_0	O07@12_0
	1772	I07_1	B07_1	O07@6_1	O07@3_1	O07@12_1
	1750	I07_2	B07_2	O07@6_2	O07@3_2	O07@12_2
	1730	I07_3	B07_3	O07@6_3	O07@3_3	O07@12_3
0.014"	1797	I14_0	B14_0	O14@6_0	O14@3_0	
	1772	I14_1	B14_1		O14@3_1	
	1750	I14_2	B14_2		O14@3_2	
	1730	I14_3	B14_3		O14@3_3	
0.021"	1797	I21_0	B21_0	O21@6_0		
	1772	I21_1	B21_1		O21@3_1	
	1750	I21_2	B21_2		O21@3_2	
	1730	I21_3	B21_3		O21@3_3	

A.2 MATLAB Source Codes

A.2.1 FFT.m

```
function FFT(y,fs,style,varargin)

nfft= 2^nextpow2(length(y));

y=y-mean(y);
y_ft=fft(y,nfft);
y_p=y_ft.*conj(y_ft)/nfft;
y_f=fs*(0:nfft/2-1)/nfft;

if style==1
    if nargin==3
```

```
        plot(y_f,2*abs(y_ft(1:nfft/2))/length(y));

        FE24O123=2*abs(y_ft(1:nfft/2))/length(y);

    else
        f1=varargin{1};
        fn=varargin{2};
        ni=round(f1 * nfft/fs+1);
        na=round(fn * nfft/fs+1);
        plot(y_f(ni:na),abs(y_ft(ni:na)*2/nfft));
    end

elseif style==2
        plot(y_f,y_p(1:nfft/2));
    else
        subplot(211);plot(y_f,2*abs(y_ft(1:nfft/2))/length(y));
        ylabel('7');xlabel('8');title('9');
        subplot(212);plot(y_f,y_p(1:nfft/2));
        ylabel('10');xlabel('11');title('12');
    end
end
```

A.2.2 EnvelopAnalysis.m

```
function Baoluo(y,fs,style,varargin)

y_hht=hilbert(y);
y_an=abs(y_hht);
    if nargin==3
        FFT(y_an,fs,style);

    elseif nargin==5
        f1=varargin{1};
        f2=varargin{2};
        FFT(y_an,fs,style,f1,f2);

    else
        error('error');
    end
end
```

A.2.3 SVM.m

```
%% Compute the discriminant function for SVMs
clear all
close all
clc

%% Preprocess the train data
```

```
load train.mat
train_data=mapminmax(data);  % Normalize
target_train=label;
[m_train,n_train]=size(train_data);

%% Hard-margin SVM
%% Constrains
f=-ones(n_train,1);
Aeq=target_train';
Beq=0;
lb=zeros(n_train,1);
ub=1e6*ones(n_train,1);

alpha0=rand(n_train,1);
options=optimset('LargeScale','off','MaxIter',1000);

%% A hard-margin SVM with the linear kernel
for i=1:n_train
    for j=1:n_train
        K_hl(i,j)=train_data(:,i)'*train_data(:,j);
        H_hl(i,j)=target_train(i)*target_train(j)*K_hl(i,j);
    end
end

[x_hl,fval_hl,exitflag_hl]=quadprog(H_hl,f,[],[],Aeq,Beq,lb,ub,alpha0,o
ptions);
med_hl=0;

for i=1:n_train
    if x_hl(i)>1e-4
        for j=1:n_train
            med_hl=med_hl+x_hl(j)*target_train(j)*K_hl(j,i);
        end
        b_hl=target_train(i)-med_hl;
        break;
    end
end

%% Implement the SVMs with the discriminant functions.
clc

%% Classify the training set
%% A hard-margin SVM with the linear kernel
sum_train_hl=zeros(n_train,1);
for i=1:n_train
    for j=1:n_train

sum_train_hl(i)=sum_train_hl(i)+x_hl(j)*target_train(j)*K_hl(i,j);
    end
    g_train_hl(i)=sum_train_hl(i)+b_hl;
    d_train_hl(i)=sign(g_train_hl(i));
end
error_train_hl=d_train_hl'-target_train;
result_train_hl=length(find(error_train_hl==0))/length(error_train_hl)
```

A.2.4 ICA_Pre-Processing.m

```
function y = ICAprepro(x) % input x is column vector;
y1 = x;
maxofarray = max(y1);
minofarray = min(y1);
heightofarray = (maxofarray - minofarray)/2;
y = y1/heightofarray;


[y2,meanvalue]= remmean(y1); % centering by remove the mean value;

y3 = y2.';    % y3 is a row vector
[E,D] = pcamat(y3);
[y4,wm,dm] = whitenv(y3,E,D); % whitening

y = y4;
```

A.2.5 ICA_Feature_Extraction.m

```
% ICA method for feature extraction (Faulty Motor Current Waveform)
% By default, there should a 4X4013 matrix as input
% Output y will be the feature of each types of waveform

function [y,A,W] = ICAfeature(x)

tic
[icasig,A,W] =
fastica(x,'g','gauss','epsilon',0.0001,'maxNumIterations',4013);
% s = W*[w1;w2;w3;w4];

y = icasig;

toc

format short

figure(8)
subplot(4,1,1)
plot(x(1,:))
title('Original Data')
subplot(4,1,2)
plot(x(2,:))
subplot(4,1,3)
plot(x(3,:))
subplot(4,1,4)
plot(x(4,:))

%  ICA Components
```

```
ICA1 = y(1,:);
ICA2 = y(2,:);
ICA3 = y(3,:);
ICA4 = y(4,:);

figure(9)
subplot(4,1,1)
plot(ICA1)
title('component 1')
subplot(8,1,2)
plot(ICA2)
title('component 2')
subplot(8,1,3)
plot(ICA3)
title('component 3')
subplot(8,1,4)
plot(ICA4)
title('component 4')
```

REFERENCES

[1] Smith, Steven W., "Chapter 8: The Discrete Fourier Transform". The Scientist and Engineer's Guide to Digital Signal Processing (Second ed.). San Diego, Calif.: California Technical Publishing. ISBN 0-9660176-3-3, 1999.

[2] M.F. Abdel-Magied, K.A. Loparo, Wei Lin, "Fault detection and diagnosis for rotating machinery: A model-based approach", Proceedings of the American Control Conference, pp. 3291-3296, June 1998 .

[3] Hasan OCAK, and Kenneth A. LOPARO, "A new bearing fault detection and diagnosis scheme based on hidden markov modeling of vibration signals", IEEE International Conference on Acoustics, Speech, and Signal Processing, vol. 5, pp. 3141-3144,2001.

[4] Hasan Ocak, and K.A. Loparo, "HMM-based fault detection and diagnosis scheme for rolling element bearings", Journal of Vibration and Acoustics, vol. 127, pp. 299-306, August 2005.

[5] Morgan electric motor sales and service's website, http://morganelectricmotors.com /motors.asp

[6] Jasminpateltech's website, http://jasminpateltech.blogspot.sg/2011_09_01_ archive.html

[7] S. Yang, "Fault detection and diagnosis of induction motors using independent component analysis", Thesis for Bachelor Degree, May 2006.

[8] Bearing data center of Case Western Reserve University seeded fault test data. http:// csegroups.case.edu/bearingdatacenter/home

[9] C.S. Chang, Z.Wang, and F. Yang, "Final Report Predictive Maintenance and Condition Monitoring of Marine Power Plant", MPA-NUS Maritime and Port Research Programme, March 2011.

[10] Steven W. Smith, "The Scientist and Engineer's Guide to Digital Signal Processing", 2nd edition, ISBN：0-9660176-3-3, 1997.

[11] N.X. Xue, "Matlab's application in digital signal processing", Qinghua University Press, 2003.

[12] Vigario,R, "Extraction of ocular artifacts from EEG using independent components analysis", Electroencephalography and clinical Neurophysiology, 103(3), pp. 395-404, 1997.

[13] Back,A. D., and Weigend, A.S., "A first application of independent components analysis to extracting structure from stock returns", International Journal of Neural System, vol. 8(4), pp. 473-484, 1998.

[14] Biswall, B.B., and Ulmer, J.L., “Blind source separation of multiple signal sources of MRI data sets using independent components analysis”, Journal of Computer Assisted Tomography, vol. 23(2), pp. 265-271, 1999.

[15] Antonini, G., Popovici, V., and Thiran, J.P., “Independent component analysis and support vector machine for face feature extraction”, Signal Processing Institute. Swiss Federal Institute of Technology Lausanne, Available from hhtp://ltsww.epfl.ch.

[16] Jolliffe, I. T., “Principal component analysis”, New York: Springer. 1986.

[17] Cardoso, J. F., “Blind signal separation: statistical principles.”, Proceeding of the IEEE, vol. 86(10), pp. 2009-2020, 1998.

[18] Vapnik, V. N., “The nature of statistical learning theory.”, New York: Springer, 1999.

[19] Chan, K, and Lee, T.W., “Comparison of machine learning and traditional classifiers inglaucoma diagnosis.”, IEEE Transactions on Biomedical Engineering, vol. 49(9), pp. 963-974, 2002.

[20] Guo, M., Xie, L., Wang, S. Q., and Zhang, J. M., “Research on an integrated ICA-SVM based framework for fault diagnosis.”, IEEE Journal, pp. 2710-2715, 2003.

[21] Min, J. H., and Lee, Y. C., “Bankruptcy using support vector machine with optimal choice of kernel function parameters.”, Experts system with application, vol. 28, pp. 603-614, 2005.

[22] Antonini, G., Popovici, V., and Thiran, J.P., “Independent component analysis and support vector machine for face feature extraction”, Signal Processing Institute. Swiss Federal Institute of Technology Lausanne, Available from hhtp://ltsww.epfl.ch.

[23] Samanta, B., “Gear fault detection using artificial neural networks and support vector machines with genetic algorithms.”, Mechanical Systems and Signal Processing, vol. 18(3), pp. 625-644, 2004.

[24] Jack, L. B., and Nandi, A. K., “Fault detection using support vector machines and artificial neural network, augmented by genetic algorithms.”, Mechanical Systems and Signal Processing, vol. 16, pp. 373-390, 2002.

[25] Yang, B. S., Hwang, W. W., Ko, M. H., and Lee, S. J., “Cavitation detection of butterfly valve using support vector machines.”, Journal of Sound Vibration, vol. 287(1-2), pp. 25-43, 2005.

[26] Yang, B. S., Hwang, W. W., Kim, D. J., and Tan, A. C., “Condition classification of small reciprocating compressor for refrigerators using artificial neural networks and support vector machines.”, Mechanical Systems and Signal Processing, vol. 19, pp. 371-390, 2005.

[27] Simon Haykin, “Neural networks and learning machines”, Third edition, Pearson education press, ISBN-13: 978-0-13-129376-2, 2009.

[28] Kuhn, H. W., and Tucker, A. W., “Nonlinear programming.”, Proceedings of 2nd Berkeley Symposium. Berkeley: University of California Press, pp. 481–492, 1951.

[29] R., Fletcher, *Practical Methods of Optimization*. 2nd ed., John Wiley & Sons, NY, 1987.

[30]Arnold Neumaier, “Complete search in continuous global optimization and constraint satisfaction.”, Acta Numerica, vol. 13, pp. 271-369, 2004.